Master's thesis

NTNU
Norwegian University of Science and Technology
Faculty of Engineering
Department of Mechanical and Industrial Engineering

Cato Seljevold

Failure Analysis of Diffusor System for Gas Turbines

Master's thesis in Mechanical Engineering
Supervisor: Afrooz Barnoush
December 2018

NTNU
Norwegian University of Science and Technology

Mjørud

Cato Seljevold

Failure Analysis of Diffusor System for Gas Turbines

Master's thesis in Mechanical Engineering
Supervisor: Afrooz Barnoush
December 2018

Norwegian University of Science and Technology
Faculty of Engineering
Department of Mechanical and Industrial Engineering

NTNU
Kunnskap for en bedre verden

Forord

Denne masteroppgaven er skrevet som en siste del av mitt integrerte masterprogram innen Produktutvikling og Produksjon ved Norges teknisk- naturvitenskapelige universitet (NTNU) høsten 2018. Oppgaven er utført i samarbeid med Mjørud AS, et engineeringfirma i Rakkestad som produserer utstyr til offshoreindustrien.

Oppgaven har bydd på mange spennende utfordringer og gode læringsmuligheter i forhold til både utmattelsesutregning av komplekse komponenter og kunnskapstilegning om bruk av forskjellige dataverktøy som kan benyttes i forbindelse med denne typen beregninger, slik som Abaqus og Link-PFAT.

Jeg ønsker først å takke veilederen min Afrooz Barnoush ved NTNU som har bidratt med verdifull kunnskap og hjelp i løpet av denne oppgaven, og koveilederen min Johan Hultqvist samt flere ansatte ved Mjørud AS som har gitt meg innsikt i historien til komponenten som er hovedtema i denne masteroppgaven.

Videre ønsker jeg å rette en stor takk til Håkon Ottar Nordhagen og Paul Qvale ved SINTEF som har bidratt med teknisk hjelp når både Abaqus og Link-PFAT har kjørt seg fast. Uten dem hadde nok simuleringen fortsatt stått og beregnet i vei.

Jeg ønsker også å takke mine foreldre Torunn og Werner som har støttet meg igjennom hele det lange masterstudiet mitt.

Sist men ikke minst ønsker jeg å rette en stor takk til min elskede samboer Sandra Sæther som har bidratt med uvurderlig hjelp igjennom hele oppgaven.

Cato Seljevold
Trondheim, 18.12.2018

Abstract

In order to reduce noise generated from a bleed air assembly in the exhaust ducts of gas turbines installed on oil- and gas platforms, a diffusor has been developed by Mjørud AS. This diffusor is designed to reduce the pressure and speed of the air being ejected by the bleed air assembly into the exhaust ducts, as the noise levels in the exhaust ducts exceeded NORSOK standards. Some problems regarding previous iterations of the diffusor has been encountered, including cracks in the welds and breaking of some components in the diffusor.

The project files of Mjørud regarding the diffusor were collected and organised in order to get a better understanding of the problems encountered with the previous iterations of the diffusor, and to be able to create a FEM model for fatigue life analysis.

In order to perform the fatigue life analysis of the diffusor, two FEM models were created. A CFD model of the air domain was created in order to evaluate the airflow in the diffusor and to collect pressure data, which was further used for the fatigue life analysis. A standard explicit model of the diffusor was created in Abaqus by recreating the production model used by Mjørud AS. This model had to be modified in order to give the diffusor the intended properties corresponding to the real-world diffusor.

Material data for both air and 316 steel had to be obtained for elevated temperatures and pressures, as the environment where the diffusor is placed has a temperature of 400 °C and the air entering the diffusor has a pressure of up to 23 bar. The material properties of the 316 steel was not readily available for such elevated temperatures and thus had to be obtained from different sources or extrapolated from previous work regarding 316 steel.

Limits to the usability of both Abaqus and the computer used for this analysis were encountered, since the models became more complex than first envisioned. This situation warranted some simplifications of the models in order to perform the analysis. The most prominent of these simplifications were the omission of the welds of the diffusor.

The fatigue life of the different components were determined during the analysis, where the component with the lowest fatigue life was found to be the top plate, which would last for 513.5 years before failure. As the calculated fatigue life of the components is not realistic, limitations of the model are discussed, and a number of ways to improve it are proposed. As the welds were omitted from the analysis, it is possible that the fatigue life of the welds will be shorter than the fatigue life of the top plate, and a fatigue life analysis of the welds is recommended for future work.

Sammendrag

For å redusere lydnivået, forårsaket av et *bleed air* system i eksoskanalene til gassturbiner installert på olje- og gassplattformer, har Mjørud AS utviklet en diffusor. Denne diffusoren ble designet for å redusere hastigheten og trykket til luften som blir sendt ut fra *bleed air* systemet og inn i eksoskanalen, siden lydnivået i eksoskanalene oversteg grenseverdiene i NORSOK's standarder. Under inspeksjon av tidligere iterasjoner av diffusoren ble det avdekket enkelte skader, inkludert sprekker i sveiser og brudd i enkelte komponenter i diffusoren.

Prosjektfilene til Mjørud AS som omhandler diffusoren ble samlet opp og sammenstilt for å få en bedre forståelse av problemene som hadde blitt oppdaget ved de tidligere iterasjonene av diffusoren, samtidig som filene ble brukt til å lage en FEM modell for å analysere utmattelse i diffusoren.

For å utføre utmattelsesanalysen ble det laget to FEM modeller. En CFD modell av luftdomenet ble laget for å analysere luftstrømmen i diffusoren, og for å samle sammen trykkdata som ble videre brukt i utmattelsesanalysen. En standard eksplisitt modell av diffusoren ble laget i Abaqus ved å gjenskape produksjonsmodellen brukt av Mjørud AS. Denne modellen måtte modifiseres for å gi diffusoren egenskaper som korresponderte med den virkelige diffusoren.

Materialdata for både luft og 316 stål ved økt trykk og temperatur måtte hentes inn siden diffusoren står i en eksoskanal med temperatur på opp til 400 °C og luften som kommer inn i diffusoren har et trykk på inntil 23 bar. Materialegenskapene til 316 stål var ikke lett tilgjengelig for slike høye temperaturer, og måtte dermed skaffes fra andre kilder og, for enkelte materialegenskaper, ekstrapoleres fra tidligere arbeid som omhandlet 316 stål.

Grensen for hva som var mulig å utføre både i Abaqus og med datamaskinen som ble brukt i denne oppgaven ble møtt, siden FEM modellene ble mer komplekse enn først antatt. Dette medførte at modellene måtte forenkles for å kunne utføre analysen, der den mest betydelige forenklingen inkluderte å utelate sveisene i diffusoren.

Levetiden til de forskjellige komponentene ble beregnet i løpet av analysen, der komponenten med den korteste levetiden var topplaten. Levetiden til denne komponenten var 513,6 år før den ville oppleve utmattelsesbrudd. Siden levetiden til komponentene ikke er realistiske, blir begrensninger i modellen diskutert, og en rekke forbedringer blir foreslått. Siden sveisene ble utelukket fra analysen, er det en mulighet for at levetiden til sveisene vil være kortere enn levetiden til topplaten, og dermed anbefales det å utføre en levetidsanalyse av sveisene i videre arbeid.

Table of Contents

List of Tables

List of Figures

Nomenclature

CDP - Compressor Discharge Pressure

FEM - Finite Element Method

FEA - Finite Element Analysis

CFD - Computational Fluid Dynamics

Operator - Company running oil platform

Diffusor - A device that hinders airflow in order to reduce the speed and pressure of an airflow.

SAE - Society of Automotive Engineers

NORSOK - Norsk Sokkels Konkurranseposisjon

Symbols

σ - Stress

ϵ - Strain

σ_a - Stress amplitude

σ_W - Fatigue limit

σ_m - Mean stress

σ_r - Stress range

$\mathbf{N}_f$ - Cycles to failure

$\mathbf{R}$ - Stress ratio

$\mathbf{R}_{p,0.2}$ - Yield strength

ν Poisson's ratio

σ_U - Tensile strength

α_L - Linear thermal expansion coefficient

Chapter 1

Introduction

1.1 History of the problem

Mjørud AS is an engineering company that among other things deliver compact exhaust- and steam systems to oil- and gas companies. In 2009 they started to develop a diffusor system that was intended to help reduce the noise levels in the exhaust ducts of a gas turbine installed on oil platforms, due to a report by Lloyd's register ODS[1], commissioned by Mjørud AS. This report found that the sound developed during normal operation exceeded NORSOK standards[2]. The source of the noise was found to be the result of among other things, improper usage of the system, which is intended to only be operated during turbine start up. When starting a gas turbine, the airflow into the combustion chamber needs to be regulated in order to not stall the turbine and allow it to spin up to operating speeds. During the period when the turbine does not need all the compressed air fed into the combustion chamber, some of the airflow is redirected before it reaches the combustion chamber through a bleed assembly which leads directly to the exhaust of the turbine. The way that the exhaust ducts were designed had the bleed air hitting the exhaust duct walls perpendicularly. Under regular operating conditions this would not have been a problem, as this was a rare occurrence, but it was later found that operators also operated the bleed air assembly to regulate the speed of the turbine during power generation to trim the speed of the turbine efficiently even though there are other systems in place that are included for this purpose, because the bleed air system is an easier system to operate.

This unintended use case meant that the bleed air assembly was in operation at a high frequency which lead to very high noise levels in the ducts. Noise levels above the recommended levels would be a hazard for the workers in the vicinity of the turbine as it could lead to an increase in the amount of hearing loss incidents. This situation would also lead to increased costs for the operators in regard to medical attention needed for their employees. Therefore, the need

for a system to reduce these noise levels are clearly needed in order to reduce the prevalence of hearing injuries and the safety of the workers.

Another intended benefit of the diffusor system was to reduce duct wear as an inspection of the exhaust ducts showed that insulation material on the inside of the ducts were eroded by the airflow. This erosion of the insulation leads to increased outside temperatures of the exhaust ducts which reduces the efficiency of the heat exchangers fitted to the exhaust since more heat is lost to the environment through the exhaust ducts. The increased temperatures could also lead to a more dangerous work environment since hot surfaces would pose a danger to the workers if they were to come in contact with these surfaces.

1.2 Initial solutions

Since several operators were experiencing high noise levels from this continuous operation of the bleed assembly, a bleed diffusor has been designed to reduce the pressure and speed of the bleed air. The bleed air is being ejected from the turbine at a pressure of upto 23 bar and temperatures up to 400 °C. This airflow travels at supersonic speeds and can critically damage the exhaust duct. The intention for this diffusor was that the airflow would be spread out over a larger surface area to reduce the speed and pressure of the airflow.

The diffusor is designed to last 20 years of normal operation before it is to be replaced during a routine check of the platform according to guidelines appropriated by Mjørud. It should sufficiently reduce the speed of the bleed air in order to eliminate damage to the insulation in the exhaust ducts. Further development to reuse the bleed air for something productive is wanted at some point, but the first requirement is to get the diffusor to a satisfactory level of robustness to be retrofitted to the systems already in place. In the following sections, the different revisions of the diffusor are presented. All information is provided by Mjørud AS.

1.2.1 Revision A

The first iteration of the bleed diffusor, shown in Figure 1.1a, was designed in October 2009 for platform EKO-J. The diffusor was designed as a 600 mm long cylinder with a diameter of 760 mm. An internal cone was added to redirect the airflow outwards through the diffusor. The cylinder walls were made from three layers of perforated plates with a thickness of 2 mm. Supporting arms were added on the outside of the diffusor to add strength to the structure. All contact surfaces between metal components were welded according to NORSOK standard M-001[3]. The intended function of this diffusor was to increase the surface area of the outgoing flow from the diffusor, and thus reduce the pressure and speed of the air entering the exhaust.

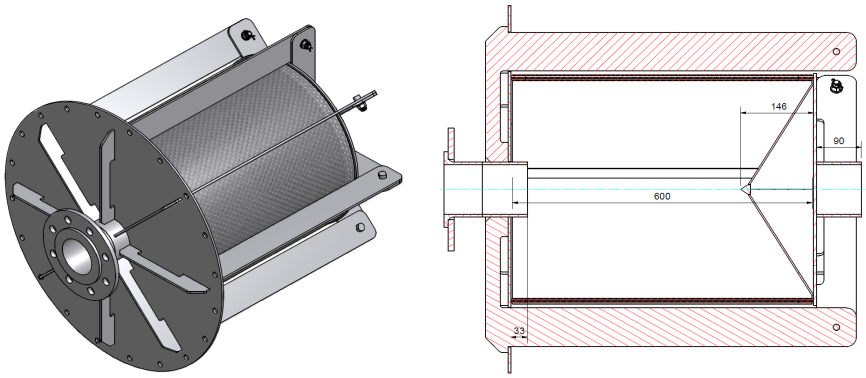

(a) Rendering of revision A of the diffusor. (b) Revision A of the diffusor, section view.

Figure 1.1: Revision A of the diffusor, gathered from the production drawings from Mjørud AS.

Problems with Revision A

Following a report by an operator that unwanted noises were emanating from the exhaust ducts, an inspection was conducted. Examination of the exhaust system and the diffusor revealed some problems with the diffusor. Some of the welds connecting the support rods were cracked and no longer functional, as shown in Figure 1.2 where it can be seen that two of the supporting rods have detached from the diffusor. In addition, the cone section inside the diffusor was flattened due to the high impact air, and thus no longer had the desired effect on the airflow.

Figure 1.2: Revision A of the diffusor after inspection. It can be seen that two of the supporting rods have detached from the diffusor and are no longer serving their intended purpose. Photo provided by Mjørud AS.

1.2.2 Revision B

The second iteration of the diffusor design, shown in Figure 1.3, was changed to alleviate the problems discovered with the first version. The support beams on the outside were changed to round rods, which were bolted, instead of welded, to the top of the diffusor. The amount of perforated plates was increased from three to four to further slow down the airflow. The cone section was removed as it would only be flattened after a short while.

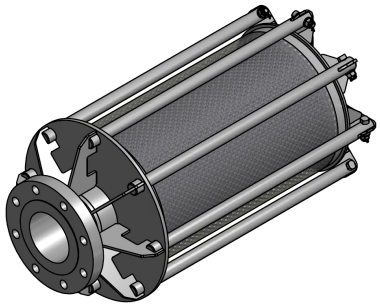

(a) Revision B of the diffusor.

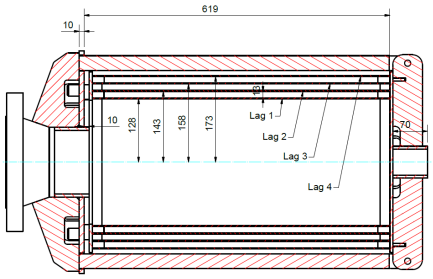

(b) Revision B of the diffusor, section view.

Figure 1.3: Revision B of the diffusor, gathered from the production drawings from Mjørud AS.

Problems with Revision B

During a routine check in 2015 of the exhaust on the platform Kristin, some new problems with the diffusor were discovered. Some cracks in the welds and perforated plates were found at the top of the diffusor where the perforated plates were fastened, as shown in Figure 1.4a. In addition, sections of the perforated plates were blown out, one of these occurrences is shown in Figure 1.4b. It was also discovered that the bolts connecting the support rods to the top of the diffusor were shaken loose, and as a result of this, the bolt holes had become oval due to motion in the fastening, as shown in Figure 1.4c.

(a) One of the cracks found at the top of the diffusor.

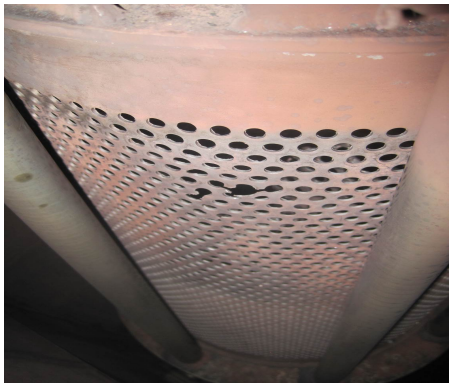

(b) One of the perforated plates with blown out section.

(c) Oval Bolt holes found in the diffusor.

Figure 1.4: Damages found in Revision B. Photos provided by Mjørud AS.

1.2.3 Revision C

The third iteration of the diffusor, shown in Figure 1.5, was improved by increasing the thickness of the perforated plates from 2 mm to 3 mm in order to increase the durability of the plates. The welds that connect the perforated plates to the top of the diffusor were changed from a butt weld to a full penetration weld to increase the durability. The support rods were again welded to the top plate to eliminate the bolted connections that were being worn in the previous iteration. To increase the durability of the weld, a groove was cut in the top of the rods to increase the weld area. The welded connection between the edges of the perforated plates were changed to full penetration welds by making welding grooves in the welding plate in order to get better welding penetration into the perforated plates and thereby increasing their durability.

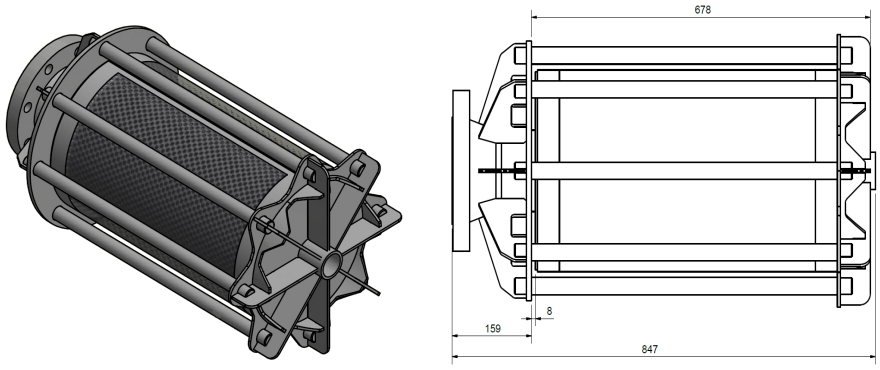

(a) Revision C of the diffusor.

(b) Revision C of the diffusor, section view.

Figure 1.5: The diffusor from revision C, gathered from production drawings from Mjørud AS.

1.3 Goal of the thesis

The main goal of the thesis is to determine the expected lifetime of the individual components of the diffusor in order to ensure that it will last the specified duration in Mjørud's internal guidelines, which is 20 years. The subject of this thesis is revision C of the diffusor. This revision is currently installed at several platforms and at the time of writing, there has not been reported any problems with this version. No calculations regarding the lifetime of the diffusor have been performed, and Mjørud AS wants to know how much wear the diffusor can take and how long they can expect it to last before they have to replace or overhaul it.

1.4 Outline of the thesis

The structure of the thesis is as follows. In Chapter 2, the theory used in this thesis is presented, including an overview of the method followed in the fatigue life analysis. In Chapter 3, the procedure followed in the thesis is presented, including a concise step-by-step guidance for analysing the diffusor model. In Chapter 4, the creation of the two FEM models is presented, where particular focus have been placed on creating the diffusor model itself. In Chapter 5, the results of the analysis is presented. In Chapter 6 the discussion of the results and further work regarding the diffusor is presented.

Chapter 2

Theory

In this chapter, the theory behind fatigue analysis will be presented, in addition to some basic principles and mechanical properties needed in order to understand the analysis.

2.1 Fatigue analysis method

In this section, the fatigue criteria utilised in this thesis is presented, along with the methodology of utilising S-N curves in order to calculate the lifetime of a component.

2.1.1 Fatigue criteria

The fatigue criterion applied in this thesis is the Mises-Sines Criterion, which is a type of multiaxial fatigue criteria where a multiaxial load case is converted to an equivalent stress amplitude. In general, these methods utilises a uniaxial stress amplitude, σ_{ar}, determined by a given function f which depends on the criterion used. The uniaxial stress amplitude is then compared with the fatigue limit, σ_W, and fatigue of the material is prescribed when σ_{ar} equals or surpasses σ_W. This behaviour is summarised in Equation 2.1, where σ_{ij} is the combination of stresses in the different dimensions.

$$\sigma_{ar} = f(\sigma_{ij}, ...) \leq \sigma_W \tag{2.1}$$

In this thesis, the Mises-Sines criterion is applied. This criterion was proposed by Sines[4], and is given in Equation 2.2,

$$\sigma_{ar} = max[\sigma_{eq,a} + MI_1] \leq \sigma_W \tag{2.2}$$

where M is the means stress sensitivity and $\sigma_{eq,a}$ is the von Mises equivalent

stress amplitude, given in Equation 2.3,

$$\sigma_{eq,a} = \sqrt{\frac{1}{2}[(\sigma_{11} - \sigma_{22})^2 + (\sigma_{22} - \sigma_{33})^2 + (\sigma_{33} - \sigma_{11})^2] + 3(\sigma_{12}^2 + \sigma_{23}^2 + \sigma_{31}^2)} \tag{2.3}$$

and the first stress invariant I_1 is given in Equation 2.4.

$$I_1 = \sigma_{xm} + \sigma_{ym} + \sigma_{zm} \tag{2.4}$$

2.1.2 Cyclic stresses and S-N Curve

A fundamental method of determining fatigue properties of materials is to subject the material to repeated loads, also known as cyclic loading. An example of a cyclic load is shown in Figure 2.1.

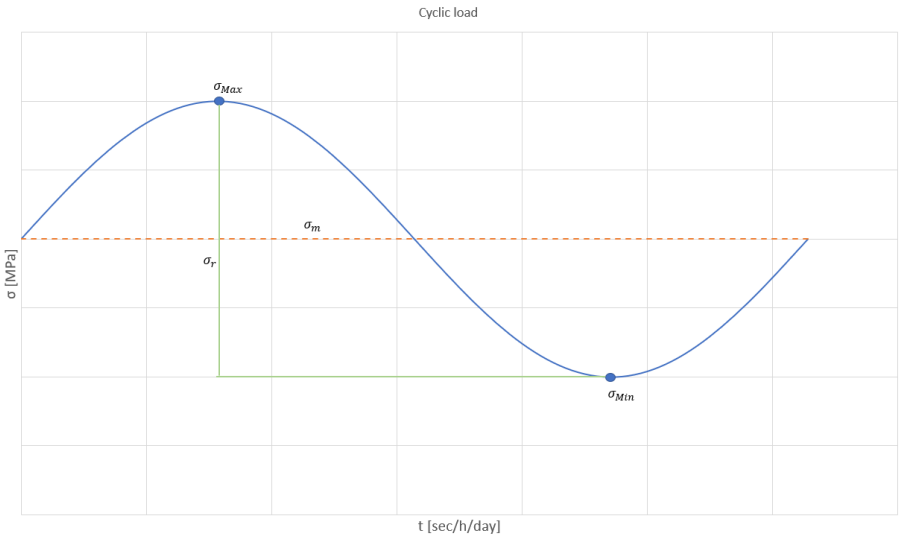

Figure 2.1: An example of a cyclic load, here the x-axis could have very different time scales depending on the load case.

From the stress-time data, one can obtain the range of stress, σ_r, which is the difference between σ_{max} and σ_{min}, shown in Equation 2.5.

$$\sigma_r = \sigma_{max} - \sigma_{min} \tag{2.5}$$

The stress amplitude, σ_a, is the range that the stress curve can vary by around the mean stress, and is given by half of the range of stress, shown in Equation 2.6.

$$\sigma_a = \frac{\sigma_r}{2} = \frac{\sigma_{max} - \sigma_{min}}{2} \tag{2.6}$$

The mean stress, σ_m, is defined as the average of σ_{min} and σ_{max}. This relation is shown in Equation 2.7 and in Figure 2.1 as a dashed line.

$$\sigma_m = \frac{\sigma_{max} + \sigma_{min}}{2} \tag{2.7}$$

The relationship between the minimum- and the maximum stress is called the stress ratio and can be obtained from the ratio between σ_{min} and σ_{max}, shown in Equation 2.8.

$$R = \frac{\sigma_{min}}{\sigma_{max}} \tag{2.8}$$

The stress ratio is included in fatigue tests as many materials exhibit different behaviour in compression than in tension. A stress ratio of R = 0 means that the specimen is only subjected to tension and a stress ratio of R = -1 would mean that the specimen is equally subjected to tension and compression during the test. The latter case is also known as fully reversed loading.

There exists some corrections to the mean stress, where the Goodman relationship is often used in order to correct the stress amplitude for non-zero mean stresses i.e. R $\neq$ -1. The Goodman relationship is shown in Equation 2.9. This relationship is known to give conservative results[5].

$$\sigma_{ar} = \frac{\sigma_a}{1 - \frac{\sigma_m}{\sigma_u}} \tag{2.9}$$

By exposing a test specimen to a sufficiently severe cyclic stress, the specimen will develop a fatigue crack or other types of damage, leading to complete failure after a given number of cycles. If another specimen of the same material is exposed to a higher stress level, the corresponding cycles to failure will be reduced. Running such tests at different stress levels for a given material and plotting the resulting cycles to failure will lead to a stress-life curve, also known as an S-N Curve, where the stress amplitude σ_a is plotted against the number of cycles to failure N_f. The cycles to failure are usually plotted on a logarithmic scale as N_f changes rapidly as σ_a decreases, and thus N_f can range over several orders of magnitude[5].

For some materials there seems to exist a limit for σ_a, where fatigue damage of the material does not occur for a stress amplitude lower than this limit under normal conditions. This behaviour is normally the case for plain carbon and low-alloy steels[5]. The stress amplitude that allows for no fatigue damage is called the fatigue limit or the endurance limit and is denoted σ_W[6]. There does not seem to exist such a limit for non-ferrous materials, since the stress amplitude shows a decreasing trend as the cycles increase, but experiments with very low stress amplitudes are not feasible due to the time it would take to observe failure of the material.

S-N curves are widely utilised in order to determine the lifetime of a material when exposed to real life conditions. An example of an S-N curve is given in

Figure 2.2. To find the expected lifetime of the material given in this example for a given stress, a horizontal line is drawn from the stress amplitude to the curve. The number of cycles is then found, and the lifetime is then calculated by multiplying this number by the time of completing one cycle. The stress amplitude defined for this kind of analysis is usually corresponding to an expected load case for the component that is being analysed.

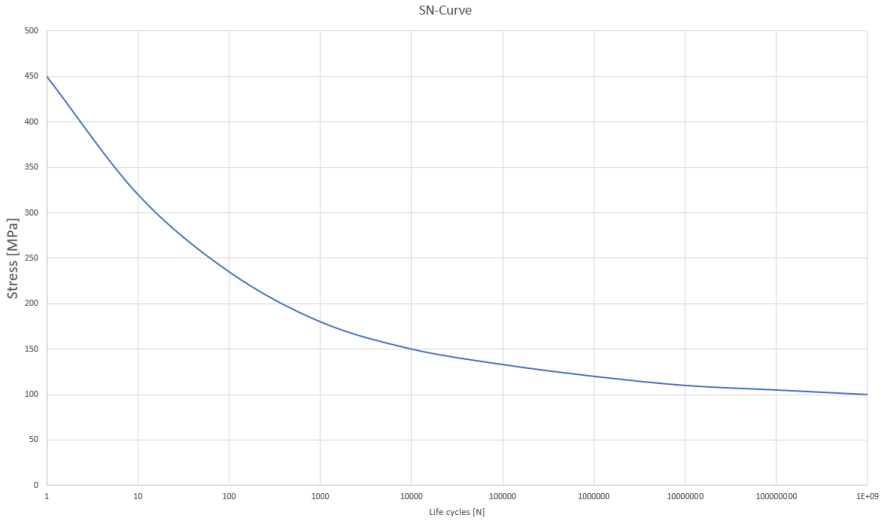

Figure 2.2: A generic example of typical behaviour of a material with a yield strength of 450 MPa.

2.2 Mechanical properties

In this section, the mechanical properties implemented in order to define the materials used in this thesis is presented.

2.2.1 Modulus of elasticity

In materials science, the modulus of elasticity is the measure of the stiffness of a solid material[6]. When stress is applied to a material, the relationship between stress and strain will initially be linear. This relationship is shown in Figure 2.3. This particular property, shown in Equation 2.10, is characterised by Hooke's law, which was discovered by Robert Hooke in 1676 using springs[7].

$$\sigma = E\epsilon \tag{2.10}$$

Here, σ is the applied stress, ϵ is the strain induced in the component and E represents the proportionality constant known as the modulus of elasticity,

Young's modulus or E-modulus of the material. The region in the deformation of the material, where the relationship shown in Equation 2.10 holds, is known as the elastic region. All deformations that take place in this region are reversible, thus the material will return to its initial size if the stresses are released.

2.2.2 Yield strength

The yield strength of a material is often defined as the value of stress where the material will no longer be able to deform elastically. Any additional stress applied to the specimen will lead to plastic deformation of the material, as shown in Figure 2.3. This type of deformation is irreversible due to plastic dissipation of energy. If a material is loaded into the plastic region and then unloaded, the plastic strain will remain while the elastic strains are recovered. It is difficult to define yielding and thus many different definitions can be found. A common definition of yield strength is the stress value that corresponds to a strain offset of 0,2%. This property is illustrated in Figure 2.3, where the dashed line represent the path of the stress strain curve if the material is loaded to the yield strength and then unloaded. This definition is often adopted for high strength steels, as they usually do not exhibit a clearly defined yield point[8].

2.2.3 Poisson's ratio

Poisson's ratio is defined as the relationship between strains in a transverse direction in relation to the primary strain induced by an applied load. In a tensile test, loads are applied in one direction, generally defined as the z-direction, and strains will thus incur primarily in this direction. Simultaneously, due to conservation of volume, this strain will introduce constrictions in the x- and y-directions as well. This relationship is shown in Equation 2.11.

$$\nu = -\frac{\epsilon_x}{\epsilon_z} = -\frac{\epsilon_y}{\epsilon_z} \tag{2.11}$$

Here ϵ_i is the strain in the i-direction, where $i = x, y, z$, and ν is the Poisson's ratio.

2.2.4 Tensile strength

Tensile strength or ultimate tensile strength, denoted σ_u is the highest level of stress a material can withstand during a tensile test. It is shown in Figure 2.3 as the highest point in the graph. When a specimen is stressed to this point, a localised deformation, called a neck, will start to form and all subsequent deformation will occur at this location. If the stress is maintained at the tensile strength, the specimen will fracture[6].

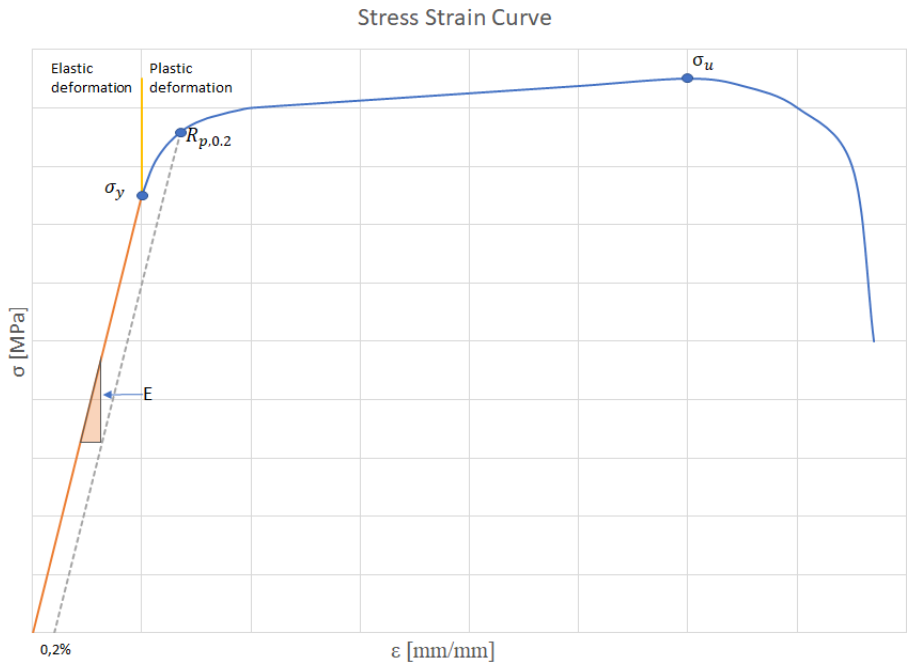

Figure 2.3: An illustration of the different mechanical properties of a material. Here Young's modulus is denoted E and represents the slope of the initial portion of the stress-strain curve. σ_y is the theoretical value for yield strength and $R_{p,0.2}$ is the yield strength adopted in this thesis. σ_u is the tensile strength of the material and is the point at which the material will exhibit breaking.

2.3 316 Steel

The material the diffusor is made of is an austenitic stainless steel with the SAE designation of 316 in the SAE steel grade system[9]. This type of steel is widely used for applications that require high temperature operation or application in areas that are susceptible to corrosion[10]. The chemical composition of the alloying elements of this steel is given in Table 2.1[9].

Chemical Symbol [Name]	Percentage composition
C [Carbon]	0.08 max
Cr [Chromium]	16.00 - 18.00
Mn [Manganese]	2.00 max
Mo [Molybdenum]	2.00 - 3.00
Ni [Nickel]	10.00 - 14.00
P [Phosphorous]	0.045 max
S [Sulphur]	0.030 max
Si [Silicon]	1.00 max

Table 2.1: Chemical composition of 316 stainless steel.

The material properties of this steel can vary depending on the composition of the alloying elements. However, despite the variations of alloying elements, there are standards in which the mechanical properties are constrained by[9]. Another factor that affects these properties, apart from alloying composition, is temperature. Since the exhaust temperature, where the diffusor is placed, is given to be approximately 400 °C, these properties had to be found at elevated temperatures. The properties that are of importance in this thesis is the Young's modulus, yield strength, Poisson's ratio and the tensile strength, which are outlined in Sections 2.2.1-2.2.4 respectively, in addition to the density of the steel.

The yield strength and the tensile strength was obtained from Desu et al.[11], and was found to be 160 MPa and 460 MPa respectively. The Young's modulus was found to be 172 kN/mm^2. Poisson's ratio was extrapolated to be 0.31. Lastly, the density was extrapolated to be 7801 kg/m^3. Extrapolation was done because the properties were not given for 400 °C in all cases of the article these values were collected from[12]. These properties are summarised in Table 2.2.

Property	Value	Unit
Young's modulus	172	kN/mm^2
Yield strength	160	MPa
Poisson's ratio	0.31	Unitless
Density	7 801	kg/m^3
Tensile Strength	460	MPa

Table 2.2: Mechanical properties defined for 316 stainless steel.

The fatigue behaviour of a test specimen made of 316 steel is presented in Table 2.3 below.

Load Ratio (R)	Stress amplitude (MPa), σ_a	Life (Cycles), N_f
0.1	334.00	4628
	290.93	17 340
	275.20	55 478
	234.33	164 938
	220.15	450 447
	180.11	1 033 948
	160.69	4 832 284
	146.45	7 893 764

Table 2.3: Fatigue data for 316 stainless steel. The data presented in this table was gathered from Mohammad et al.[13].

The fatigue test performed by Mohammad et al.[13] was performed with the specimen at room temperature. When in operation, the diffusor has a temperature of about 400 °C, and one could suspect that the fatigue life of the component would be affected by this increased temperature. However, according to a review article by Omesh K. Chopra[14], the fatigue life of austenitic stainless steel is not affected by temperatures up to 427°C and thus the fatigue data gathered from Mohammad et al.[13] was considered valid for this thesis.

2.4 Finite Element Method

In this age of increased computing power, one method of calculating various component responses when subjected to different load cases is the Finite Element Method, abbreviated to FEM. This method solves problems of structural mechanics by dividing a problem into smaller and simpler domains with easier solutions. The larger part is divided using 1D, 2D or 3D elements. 1D elements are beam elements which act as a thin beam connecting two nodes together. 2D and 3D elements are continuum elements, where 2D continuum elements act as a film or a shell wrapping around a part, connecting three or more nodes together. The 3D continuum elements are positioned such that they accurately represent the shape of the component by connecting four or more nodes together. There are many element types utilised in FEM, where the most important difference is the number of nodes used to form the element. Utilising elements with a larger amount of nodes leads to a larger amount of equations needed to be solved in order to run the simulation, but in many cases a higher amount of nodes gives more precise results. An example of a ten noded tet-element is shown in Figure 2.4.

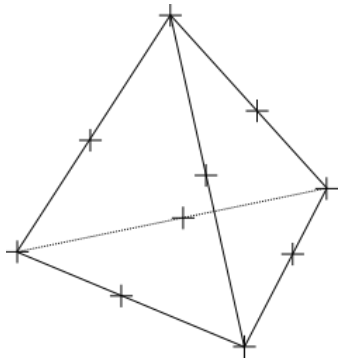

Figure 2.4: A 10-noded tet element used in the simulation, where the 10 nodes are shown with crosses.

The relationship between the displacement of the nodes $\mathbf{v}$ and the nodal forces $\mathbf{S}$ describes the behaviour of the individual beam elements[15]. This relationship is shown in Equation 2.12,

$$\mathbf{S} = \mathbf{kv} \tag{2.12}$$

where $\mathbf{k}$ is the stiffness matrix of the element, which is established by standard structural principles. When the element behaviour is determined, the elements need to be assembled into a system, which is done by requiring kinematic compatibility and static equilibrium at all nodes. For the more complex cases such as 2D and 3D elements, it is necessary to make sure that the continuity requirements along the element borders, such as edges and surfaces, are satisfied as a

consequence of compatibility at the nodes. This assembly process leads to the system stiffness relation, shown in Equation 2.13.

$$\mathbf{Kr} = \mathbf{R} \tag{2.13}$$

Here, $\mathbf{K}$ is the system stiffness matrix, $\mathbf{r}$ is the nodal point displacement in vector form and $\mathbf{R}$ is the nodal forces in vector form[15]. The size of the matrices is dependent on the amount of elements in the model and determines how many equations that have to be solved, and thus the amount of work required from the computer increases with the amount of elements.

2.5 Thermal expansion

When a material is subjected to an increase in temperature, it expands due to an increase of the average molecular kinetic energy of the material, and thus the molecules maintain a greater separation[5]. When determining the thermal expansion of a material, linear expansion is often considered, and thus a linear coefficient of expansion is needed[6]. To find this coefficient, a thin bar is used to measure the strain induced at different temperature changes, this relation is shown in Equation 2.14.

$$\frac{\Delta L}{L} = \alpha_L \Delta T \tag{2.14}$$

Where ΔT is the change in temperature ($T_{final} - T_{initial}$), α_L is the linear thermal expansion coefficient and $\frac{\Delta L}{L}$ is the strain measured in the sample. A cyclic temperature fluctuation will lead to cyclic strains in the component and can thus contribute to fatigue if the strains are of a large enough magnitude[5].

Chapter 3

Method

In this chapter, the procedure followed during the thesis is presented.

3.1 Information gathering

In order to perform an adequate analysis of the diffusor, correct information about the problem had to be obtained. At the start of the thesis work, two weeks were spent at Mjørud AS in order to collect and organise data about the problems encountered with the diffusor. As Mjørud has had problems with the diffusor and surrounding systems before, there exists a lot of documentation about the earlier failures as introduced in Section 1.2. This documentation had to be organised as many people had worked on the solution of this problem, and there was no orderly system in place. The company had also hired Lloyd's register ODS to look at some earlier behaviour of the diffusor and the airflow inside it[16]. The end results of their report were incorporated as some of the boundary conditions in the model. These values will be presented in Section 4.3.2. The model, created in Abaqus, was based on the 3D-production model used by Mjørud AS as previously displayed in Figure 1.5a in Section 1.2.3.

3.2 FEM Simulation

In this section, a short and concise presentation of the steps taken in order to perform the lifetime analysis of the diffusor is presented.

1. The model was imported as a step-file in order to recreate the geometry of the diffusor. It was discovered that the step file was not accurate enough, as some parts intersected in the model. Therefore, the step file was instead treated as a guide in order to recreate the diffusor in its entirety using the built-in modelling tools in Abaqus. An air domain was created by using the diffusor geometry to cut a hole in a cylinder in order to define the volume where the air will flow.

2. Since the model was symmetrical about the two principal planes XZ and YZ, this symmetry was utilised in order to decrease the size of both the diffusor model and the air domain by three quarters, and therefore decrease the computation time substantially.

3. The air domain model was prepared for Computational Fluid Dynamics (CFD) analysis by defining:

    - The boundary conditions of the airflow such as pressure, temperature and velocity.
    - The properties of the air used in the simulation such as density, temperature and viscosity.
    - Step parameters such as total time, initial step length and solvers to be included.

4. The air domain model was meshed using tetrahedral elements.

5. The simulation was executed on a dedicated simulation computer with an Intel Xeon, 4-core processor and 16 GB of Memory.

6. The results from the air domain simulation were collected and processed in Excel.

7. The processed results from the air domain model were defined as new boundary conditions for the loads in the diffusor model.

8. The diffusor model was prepared for standard explicit analysis by defining:

    - The boundary conditions obtained from the processed results of the CFD analysis. These boundary conditions included the pressure applied to the perforated plates and the top plate.
    - The properties of the steel used in the diffusor, such as Young's modulus, yield stress and density.
    - Step parameters such as total time, initial step length and step type.

9. The diffusor model was meshed in a similar manner as the air domain using tet-elements.

10. The simulation was executed on the same computer as was utilised for the air domain model.

11. The resulting file from the diffusor model simulation was imported to a post-processor supplied by SINTEF called Link-PFAT[17].

3.3 S-N Curve methodology in Link-PFAT

In Link-PFAT, there are several different methods of failure analysis available to the user in order to calculate the lifetime of the diffusor. The analysis type utilised in this thesis was the local stress mode, where the life prediction is based on the equivalence between the point in the model with the highest stress and a standard smooth fatigue specimen under the same local stress[18]. This method is the same as the one outlined in Section 2.1.2.

Some material parameters for the 316 steel had to be entered into Link-PFAT in order to perform the lifetime calculations, including data to create an S-N curve. The data imported in order to define the S-N curve is given in Table 2.3 in Section 2.3.

The multiaxial criterion to be applied in Link-PFAT was Sines criterion as outlined in Equation 2.2 in Section 2.1.1. The mean stress model defined for this analysis was the Goodman model[19], as presented in Section 2.1.2.

Chapter 4

Finite Element Method model

In this chapter the creation of the FEM model will be described in detail, along with some background information about the different programs used during the analysis.

4.1 Software used in the analysis

4.1.1 Autodesk Inventor

The program used in order to model the diffusor by Mjørud AS was Autodesk Inventor. This program is a commercial CAD tool adopted by many companies that develop new products and offers a full suite of engineering and design tools to the user[20]. In this thesis, Autodesk inventor was utilised in the information gathering stage since the 3D-model had to be accessed in order to export it as a step file into Abaqus for further analysis.

4.1.2 Abaqus 6.14

The main body of work in this thesis was done with Abaqus version 6.14[21]. The program is mainly applied in order to simulate different types of systems including mechanical-, electrical- and fluid systems in order to predict mechanical responses or airflow behaviour, among other things. The module of Abaqus utilised in this thesis was mainly the CFD module in order to compute the airflow through the diffusor and the standard module in order to calculate the mechanical response of the diffusor from the resulting loads of the airflow.

4.1.3 Link-PFAT

The post-processor Link-PFAT is a program developed by SINTEF. In this thesis it was used to easier process the data from the results of the Abaqus simulation. The programme follows the same method as explained in section 2.1.2, regarding extrapolating cycles to failure using S-N curves.

4.2 Diffusor model

In the following sections, the creation of the diffusor model will be presented. Figure 4.1 is included here in order for ease of reference and to give the reader a better understanding of the placement of the components in the diffusor. This illustration was made prior to any changes to the model outlined in the following sections.

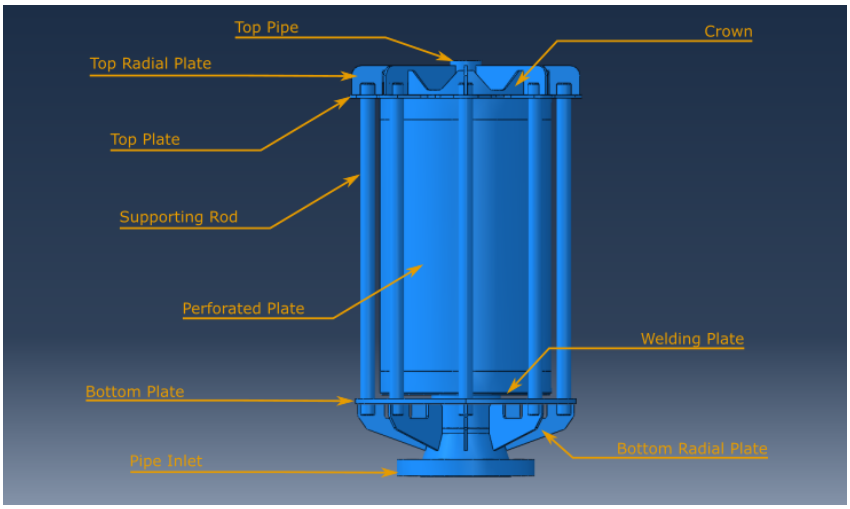

Figure 4.1: An illustration of the naming scheme adopted in this thesis for the different components that the diffusor is made up of.

4.2.1 Creating the model

The diffusor model was first imported directly from the CAD files that Mjørud had developed for the diffusor. This process was done by exporting the CAD assembly as a step file from the Mjørud database, and importing it into Abaqus. However, some modifications had to be made on this model, as it was intended to be used for production and not for analysis. In the following subsections, the creation of the main parts of the diffusor model will be explained. The three main parts that needed some changes were the perforated plates, the supporting rods and the top plate. Minor changes were made to the crown piece and the welding plate. These components are shown in Figure 4.1 above.

Perforated plates

The perforated plates in the diffusor from the CAD-files were modelled with an outline of where the perforations should be on the plate, without defining the actual holes in the model. This lack of detail was a problem since no air could pass through the perforated plates in the simulation and thus the results of the simulation would not correspond to the real-world diffusor. The CAD assembly, together with the specifications for the hole spacing included in the drawing for the diffusor, was utilised in order to create new perforated plates that would function as intended in the simulation.

The specifications of hole size and spacing is shown in Figure 4.2, and since the outline of the area supposed to have holes were known, the total area of holes could be calculated approximately so that the correct number of holes could be made in the perforated plates.

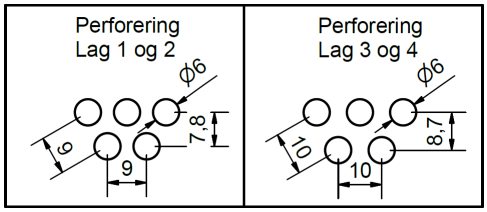

Figure 4.2: The specifications of the holes in the perforated plates, where Lag 1 og 2 corresponds with the two innermost plates and Lag 3 og 4 corresponds with the two outermost layers. This specification is included in the production drawing from Mjørud AS.

This configuration of holes can be represented by a parallelogram for the two different layer layouts, where the holes are placed in the four corners. The area of the holes that overlap the parallelogram will in total be equal to the area of one hole, as displayed in Figure 4.3, as the internal angles of a parallelogram totals 360°. This similarity is exploited when calculating the percentage of the area that is occupied by holes.

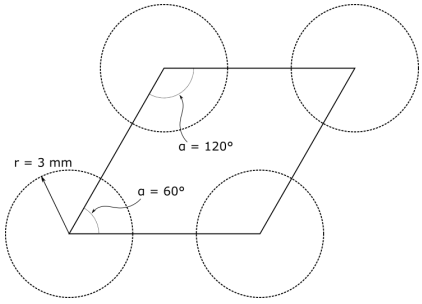

Figure 4.3: The parallelogram with overlapping holes.

Applying the formula for the area of a parallelogram on the two different layouts, given in Equation 4.1 and 4.2, and the formula for the area of a circle, given in Equation 4.3, the percentage of the area of the perforated plates that should be occupied by holes could be calculated using Equation 4.4.

$$A_1 = b_1 h_1 = 9 \text{ mm} \cdot 7,8 \text{ mm} = 70,2 \text{ mm}^2 \tag{4.1}$$

$$A_2 = b_2 h_2 = 10 \text{ mm} \cdot 8,7 \text{ mm} = 87 \text{ mm}^2 \tag{4.2}$$

$$A_h = \pi R^2 = \pi \cdot (3 \text{ mm})^2 = 28,27 \text{ mm}^2 \tag{4.3}$$

$$h_{\%} = \frac{A_h}{A} \tag{4.4}$$

Using the numbers specified in the drawing, the percentages of the area covered by holes for layer 1 and 2 were calculated to be 40%, and for layer 3 and 4 the percentages were calculated to be 32.5%. These values are presented in Table 4.1.

The holes are not distributed along the entire perforated plate, but a section on the face of the perforated plate is defined in the drawings where the holes should be placed. This area is termed the *drawing area* and can be seen in Figure 4.4a as the outline drawn on the face of the cylinder. The total area of the plate and the drawing area were calculated using measurements taken from the imported step files, and the results are shown in Table 4.1.

Layer	Area [mm^2]	Drawing Area [mm^2]	$h_{\%}$
1	490 088.5	405 600	40%
2	546 637.1	448 974	40%
3	603 185.8	506 064	32.5%
4	659 734.5	547 328	32.5%

Table 4.1: Data extracted from the CAD files in order to calculate the area occupied by holes.

These values were further utilised in order to calculate the *hole area*, which is the total area occupied by holes in the plates. It is important to calculate the correct total number of holes in each plate so that the total area that the air can flow through matches the physical diffusor in order to ensure that the perforated plates have the correct airflow resistance as intended by Mjørud. This calculation was done by utilising the calculated area of a single hole given in Equation 4.3. The results of these calculations are shown in Table 4.2.

Layer	hole area [mm^2]	# holes
1	162 240.0	5739
2	179 589.6	6353
3	164 470.8	5818
4	177 881.6	6292

Table 4.2: The parameters calculated in order to determine the number of holes in each plate.

Since Abaqus does not allow modelling of a flat plate and then rolling it into a cylinder, the holes needed to be placed equally spaced around the plates in a specific pattern. The length of the hole areas of the individual plates were measured from the step files.

$$\begin{gathered}(hole\ diameter) + n \cdot (hole\ distance) = (length\ of\ hole\ area) \\ n = \frac{(length\ of\ hole\ area) - (hole\ diameter)}{hole\ distance}\end{gathered} \tag{4.5}$$

Equation 4.5 was used to determine the number of holes on a single row of holes. Since the holes are placed in rows with alternating lengths, where the longer row has one more hole than the shorter row, it was decided that the number of holes determined by Equation 4.5 would be adopted for the short row of holes that is placed between the longer rows. Thus, the longer rows would have $n+1$ holes. In order to calculate the number of rows in the plates, these values were input into Equation 4.6, where it is assumed that there is one more long row than short row. The variable x is the number of long rows.

$$(n+1) \cdot x + n \cdot (x-1) = \#holes \tag{4.6}$$

Solving for x gives the number of long rows needed in order to include the correct number of holes, given n holes in the short rows. This operation is shown in Equation 4.7.

$$x = \frac{\#holes + n}{2n+1} \tag{4.7}$$

The values for x and n were calculated for all four perforated plates and the results are shown in Table 4.3 below.

Layer	Holes Long row	Number of Long Rows	Holes Short rows	Number of Short Rows	Holes Total
1	58	50	57	49	5693
2	57	56	56	55	6272
3	53	56	52	55	5828
4	51	63	50	62	6313

Table 4.3: The summarised hole information about each plate.

Note that the total number of holes are not exactly the same as the ones given in Table 4.2, but the closest possible with these calculations and approximations. Since some of the calculations for numbers of holes in a particular row resulted in n being a non-integer, it had to be rounded to the nearest integer. This rounding led to the length of the hole area being slightly different from the drawing, by up to 3 mm at the most. The same type of rounding error was encountered when calculating the number of rows in the plates, where the largest error was a difference of 81 holes. The distribution of the holes is simplified by ignoring the welding seam in the plate and placing the holes equally spaced around the whole cylinder.

One of the original perforated plates is shown in Figure 4.4a. The updated plate utilised in the simulation with the modelled holes is shown in Figure 4.4b. There are four perforated plates in total, with similar construction, but with different diameters.

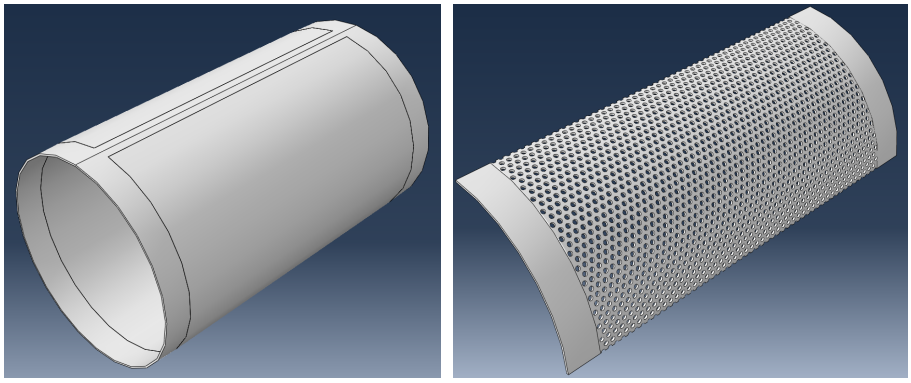

(a) The original perforated plates used by Mjørud.

(b) The modified perforated plates used in the analysis.

Figure 4.4: The modifications made in order to accurately represent the perforated plates.

Supporting rods

The supporting rods are the eight rods running alongside the diffusor and are the only parts linking the inlet of the diffusor to the top. These rods run through holes in both the bottom plate and the top plate. When they were imported directly from the step files, some intersections between the rods and the top- and bottom plate were detected as the clearances were very small. Since this would lead to the simulation not being able to run, this issue had to be addressed. Thus, the rods had to be modelled as new parts in Abaqus. As these rods are not particularly complex in their construction, they were easily recreated, however, clearance between the parts had to be ensured so that the simulation could run without problems. One of the original rods can be seen in Figure 4.5a, and the modified rod in Figure 4.5b. It can be seen that the changes made were not significant since the only feature that has been removed is a chamfer at both ends of the rods. The rods have also been partitioned near the notches in order to get a better mesh generated for the rods, and to be able to easier attach them to the top- and bottom plate. This partition of the supporting rods is shown in Figure 4.5b as the lines near the ends of the supporting rods.

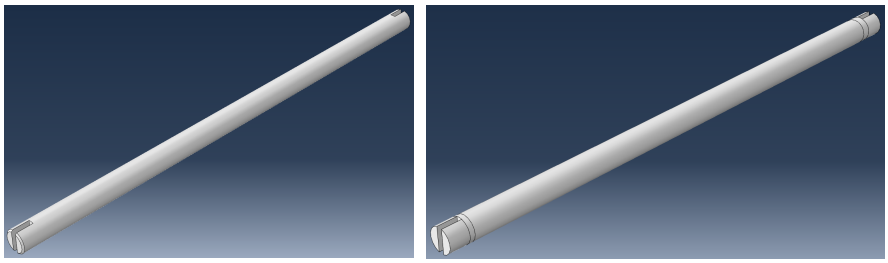

(a) The original supporting rod used by Mjørud.

(b) The modified supporting rod used in the analysis.

Figure 4.5: The modifications made in order to simplify the supporting rods.

Top plate

The plate at the top of the diffusor, where both the supporting rods and the perforated plates are attached, has a particularly complex shape along the outer edge and required some careful modelling in order to recreate the original design. Since the detailed drawing of this component was not included in the gathered files from Mjørud, the new component, made in Abaqus, had to be made with measurements performed on the imported step file. The shape of the top plate was recreated as closely to the original as possible using curves and circles drawn on top of the old component. The original top plate is shown in Figure 4.6a and the updated quarter of the top plate utilised in the simulation is shown in Figure 4.6b. The lines at the face of the updated plate are partitions of the part where the perforated plates are supposed to be attached, similarly as was done with the supporting rods.

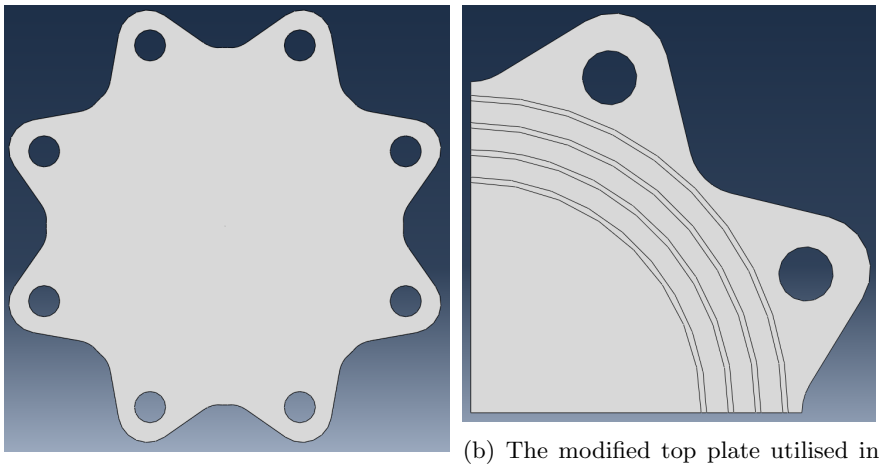

(a) The original top plate used by Mjørud.

(b) The modified top plate utilised in the analysis.

Figure 4.6: The modifications made in order to simplify the top plate.

Welding plate

The production model was modelled without welds, and only included information about what kind of welds that were needed on the different parts. Because of this simplification of the production model, some sections of the diffusor had to be changed in order to give it the correct function in the model. The part termed the welding plate, which has been developed in order to support the four perforated plates and hold them together, is shown in Figure 4.7a. This plate is modelled with grooves where the perforated plates are supposed to be welded to the welding plate in the original drawing. The reason for including these grooves is in order to get easier access to the weld and to get better weld penetration into the perforated plates. In the diffusor model this plate was replaced with a closed plate, as this will be the end result after welding, and the perforated plates needed a surface to be attached to. This modified plate is shown in Figure 4.7b.

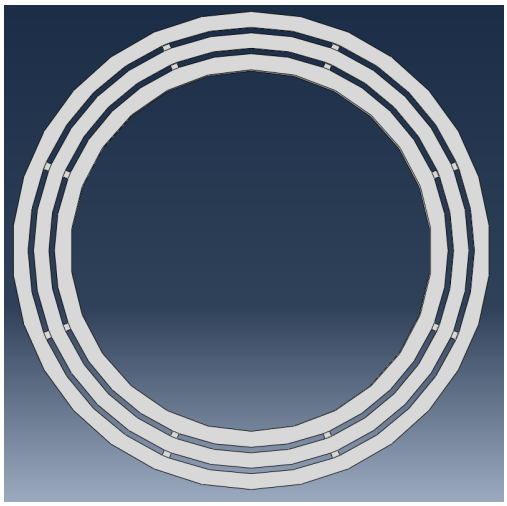

(a) The original welding plate used by Mjørud.

(b) The modified welding plate utilised in the analysis.

Figure 4.7: The modifications made in order to simplify the welding plate.

Crown

The circular piece at the top of the diffusor, called the crown, which is attached to the top plate and the top radial plates, had to be remade in Abaqus. The reason for this requirement was due to collisions between the crown and the top radial plates being detected in Abaqus. The crown and the top radial plates are attached with a half-lap joint, which was also where the collisions were detected. The crown has a complex curve to it, and since no detailed drawings of this component was found, it was decided to simplify the crown piece. The crown was made to be a simple band with grooves for the half-lap joint and the complex curve was not included. The original design for the crown is shown in Figure 4.8a and the modified crown is shown in Figure 4.8b

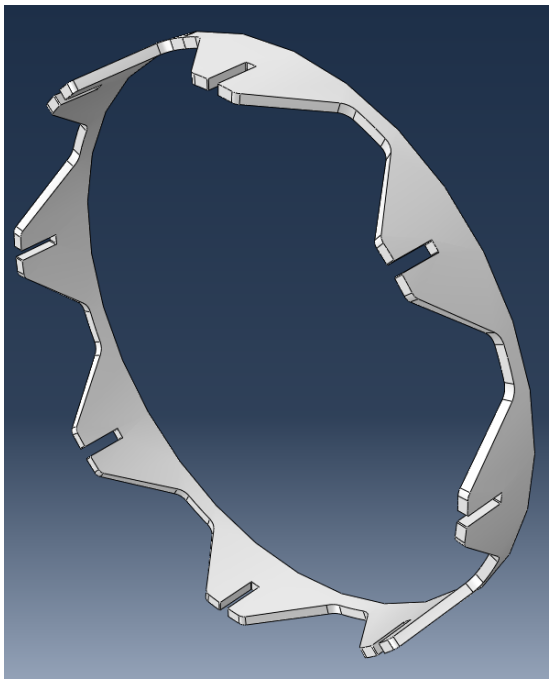

(a) The original crown piece used by Mjørud.

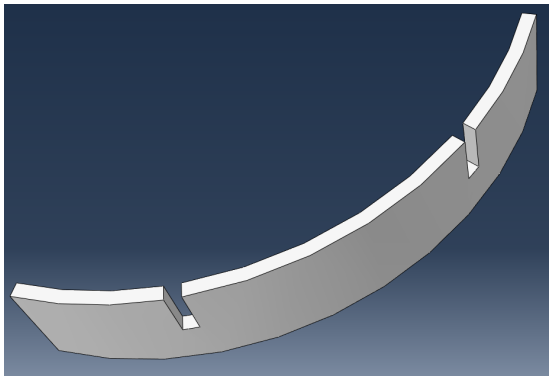

(b) The modified crown piece utilised in the analysis.

Figure 4.8: The modifications made in order to simplify the crown piece.

4.2.2 Assembly of the model

In order to perform a simulation with the diffusor, the parts of the diffusor were assembled together in the Abaqus assembly module. The individual components of the diffusor were attached to each other by utilising tie constraints, which means that the parts would be rigidly attached to each other. This attachment

method was executed instead of modelling individual welding seams where the diffusor would be welded. This simplification was done as the goal of the thesis is to examine the different components of the diffusor, and not the welds as they were assumed to hold during the operation of the diffusor. The finished model is shown in Figure 4.9.

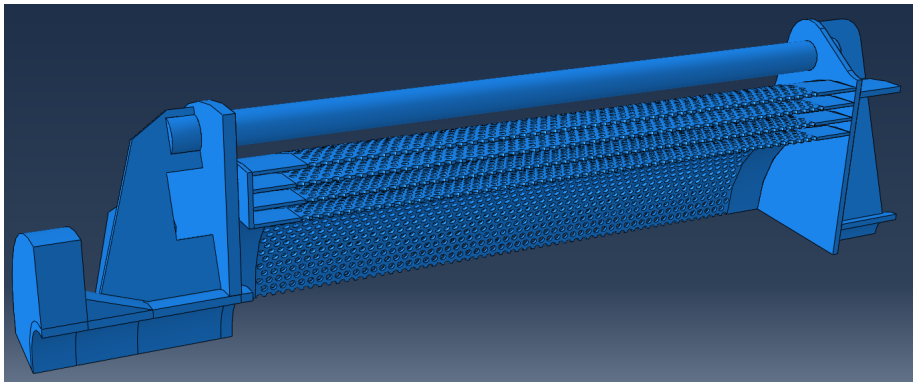

(a) Internal view of the diffusor model.

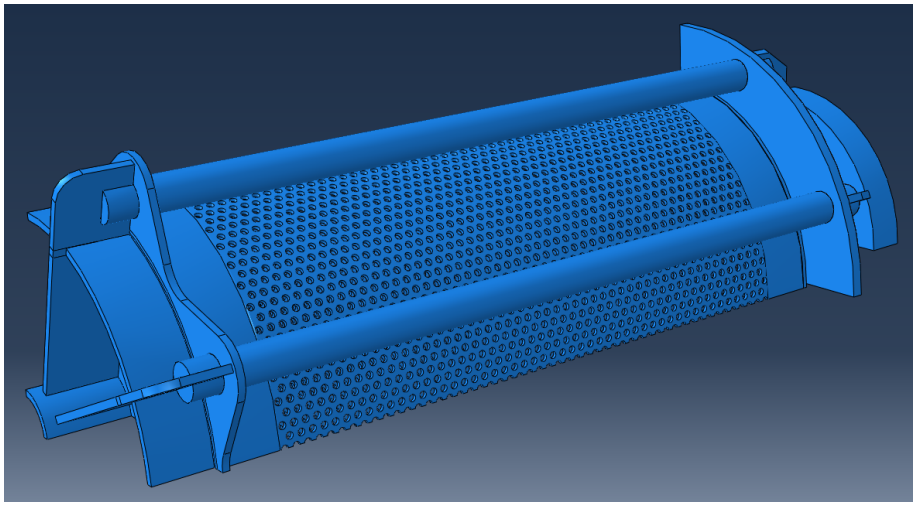

(b) External view of the diffusor model.

Figure 4.9: The finished model of the diffusor.

4.2.3 Setup of the simulation

In this section, the different parameters specified for the diffusor simulation will be presented.

Material

The diffusor is completely comprised of 316 Stainless steel as per specification in the drawings provided by Mjørud and in accordance with NORSOK M-001[3]. This particular stainless steel is often chosen for components placed in maritime environments due to its good resistance to corrosive elements found in such environments. The properties of 316 steel defined in the simulation is shown in Table 4.4 below. Note that not all the available mechanical properties for 316 steel is used in the simulation and thus only the ones relevant for this simulation will be shown here. These properties have already been introduced in Section 2.3.

Property	Value	Unit
Young's Modulus	172	kN/mm^2
Yield strength	160	Mpa
Poisson's ratio	0.31	Unitless
Density	1 781	kg/m^3

Table 4.4: The mechanical properties defined in this simulation for 316 Stainless steel.

Mesh

The mesh generated for this simulation was a tetrahedral mesh, where ten-noded tetrahedrons were defined as the elements of the mesh. This type of mesh element was selected primarily in order to get the components to be meshed properly without needing a lot of partitioning of the individual components. The default elements assigned in Abaqus is quad elements, which are quadratic bricks and are in some cases better suited for FEM analysis[22], but as these elements are not always suited for complex components, tet elements were chosen instead. An example of a tet-element is shown in Figure 2.4 in Section 2.4. The entire model was meshed with the goal of having elements of approximately 1 to 3 mm in length between nodes as this would give a good resolution of the mesh for the entire model. Some of the larger parts, such as the pipe inlet, would probably not have needed to be meshed with such a fine resolution, but could have been partitioned and given a larger mesh, however this method could also lead to less accurate results of the simulation. The mesh of the model is shown in Figure 4.10 below.

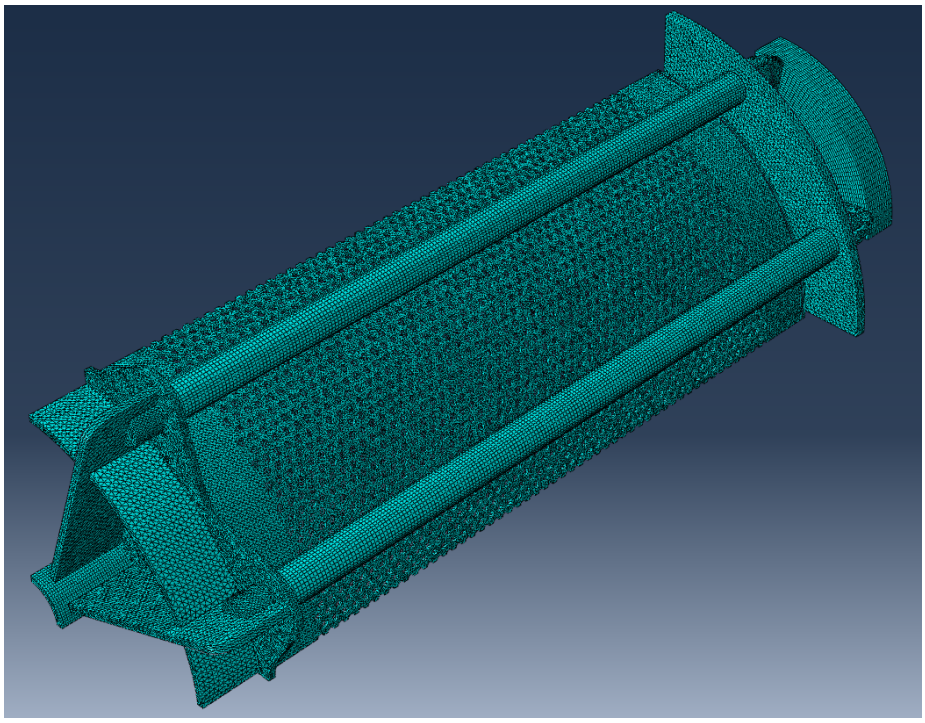

Figure 4.10: The mesh generated for the diffusor model.

Step definition

The step parameter defined in this simulation was a dynamic explicit step. The step increment was set to be automatic, so that Abaqus would decide what increment length would be sufficient in order to get converging results. The option for non-linear geometry was enabled in case the model experienced large deformations, despite that this behaviour was not expected.

Load case and boundary conditions

The load case of this simulation was extrapolated from the results of the CFD analysis, which will be presented in Section 5.1. The pressure readings from the CFD model was collected from several components that were deemed to be failure risks, both from the initial overview of previous diffusors and from the results of the CFD simulation. The parts that were selected were the perforated plates and the top plate. The pressure values were collected from several spots for each component, the maximum values during the simulation were identified at each of these spots and these values were averaged in order to create a representation of a uniform pressure acting on the part. These pressure values are shown in Table 4.5 below. An amplitude was defined in Abaqus so that the pressure loads would be gradually increased up to their maximum values.

Part Name	Pressure [MPa]
Perforated plate 1	0.149
Perforated plate 2	0.131
Perforated plate 3	0.119
Perforated plate 4	0.108
Top Plate	0.252

Table 4.5: The pressure values set as an average pressure acting on the different parts in the simulation.

The boundary conditions of the simulations were that the mounting surface of the inlet on the diffusor would be fixed in all directions, and thus unable to move during the simulation.

4.2.4 Optimisation of the model

Since the initial attempt of running the simulation resulted in Abaqus returning an error code regarding too many elements in the model, some optimisations had to be made. The fact that the diffusor was symmetrical about two planes was a reasonable place to start. The diffusor model was reduced by three quarters of the elements by utilising the symmetry planes xz and yz. This model reduction led to the model being made up of significantly fewer elements and thus solved the matter regarding the high number of elements. All the figures displaying the different updates of the components are shown after this symmetry had been utilised.

4.2.5 Approximations and simplifications of the model

Since the diffusor is placed inside the exhaust duct of the gas turbine system, the temperature of the diffusor will be at approximately 400°C during operation. The diffusor would experience cyclical thermal stresses when the gas turbine is powered down and no combustion occurs, but this situation was considered to be a relatively rare occasion compared to the high frequency of the air being pushed through the diffusor. Thus the thermal stresses was not considered to have a significant impact on the lifetime of the diffusor and therefore not considered here. It was also discovered that the fatigue life of austenitic stainless steel in air was independent of temperature up to 427 °C[14]. However, since the diffusor had been heated to such a high temperature, the mechanical properties for the steel had to be used at these temperatures.

Since the welds were not included in the analysis of the diffusor, the components of the diffusor could be attached to each other in Abaqus by using tie constraints where the contact surfaces of two components are attached together by binding the nodes of the meshes together.

4.3 CFD model

In the following sections, the creation of the CFD model is presented.

4.3.1 Creating the model

In order to create the CFD model, an accurate representation of the volume that the air is flowing through is needed. This representation was created by modelling a cylinder that encompassed the entire diffusor. Then the diffusor model was defined as a cutting tool in order to create an inverse of the diffusor. Since this method would create an exact representation of the volume that the air flowing through the diffusor would occupy, no other changes were needed in order to get an accurate model. The CFD model is shown in Figure 4.11a below, and a transparent view is included in Figure 4.11b in order to give a better view of the CFD model.

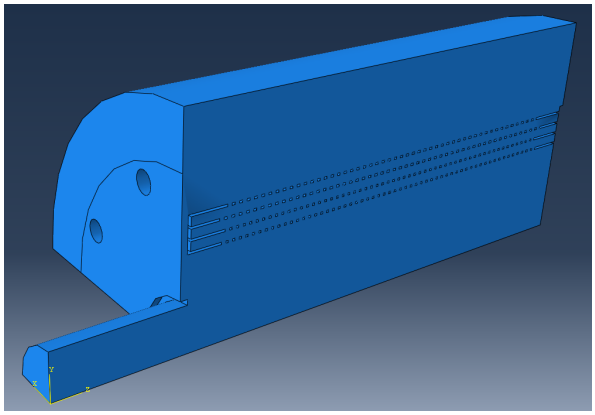

(a) The finished CFD Model.

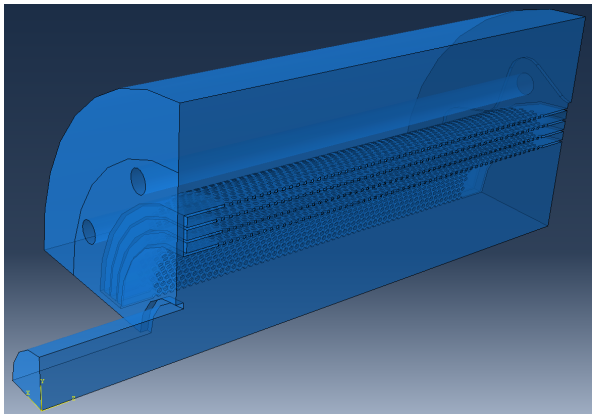

(b) Transparent view of the CFD model.

Figure 4.11: Solid and transparent view of the CFD model.

4.3.2 Setup of the simulation

In this section, the different parameters specified for the CFD model will be presented.

Material

Since the diffusor is placed at the end of a bleed system from a combustion chamber on a gas turbine, the gasses flowing through it will be a mixture of CO_2, air and possibly a small amount of uncombusted fuel, but the chemical composition of these gasses will not have any significant impact on the model, so it was decided that the airflow should be simplified. The gas is therefore treated as being comprised of only hot air, and thus only the material properties of air were needed. These properties are shown in Table 4.6 for the particular pressure and temperature at the inlet of the diffusor, namely 400°C and 0.25 MPa. As already mentioned, these pressure and temperature values were obtained from the report by Lloyd's register ODS[16], provided by Mjørud AS. The density of air at this temperature and pressure was obtained from The Engineering Toolbox[23]. The specific heat of the air was obtained from an article by Hilsenrath et al.[24]. The thermal conductivity was obtained from The Engineering Toolbox[25].

Property	Value	Unit
Density	1.331	Kg/m^3
Dynamic viscosity	$32.4 \cdot 10^{-6}$	Pa·s
Temperature	400	°C
Specific heat	1.063	kJ/(Kg·K)
Thermal conductivity	$50.48 \cdot 10^{-3}$	W/(m·K)

Table 4.6: The properties used to define the material incorporated in the CFD model. These values are specified for a temperature of 400 °C and a pressure of 0.25 MPa.

Mesh

The mesh generated for the CFD model was a tetrahedral mesh, where ten-noded tetrahedrons are used in order to accurately represent the component. This element assignment was defined in order to avoid having to partition the CFD model, as the other element types available in Abaqus would require partitioning of the model as it was too complex to mesh. The mesh size was kept at approximately 3 mm around the fine details of the diffusor in order to accurately represent the smaller parts of the CFD model, such as the holes in the perforated plates. This size limitation led to a very fine mesh for some of the

larger regions of the model as well, but the only disadvantages with this situation would be some added computation time. The finished mesh of the CFD model is shown in Figure 4.12a below, and a transparent view in order to give a better overview of the mesh is shown in Figure 4.12b.

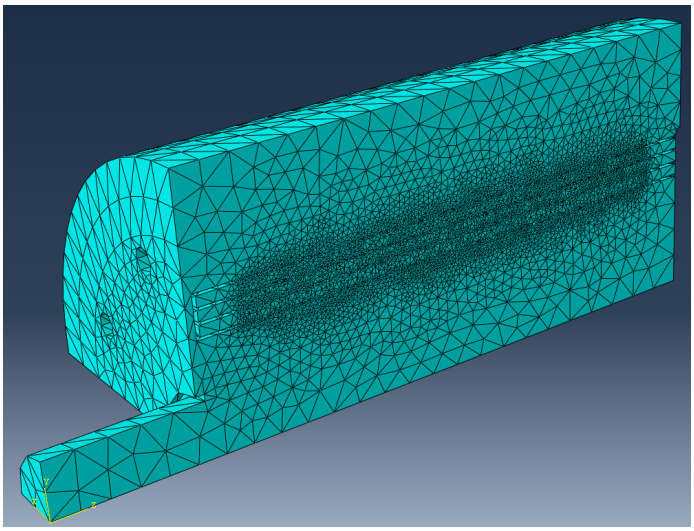

(a) The mesh of the finished CFD Model.

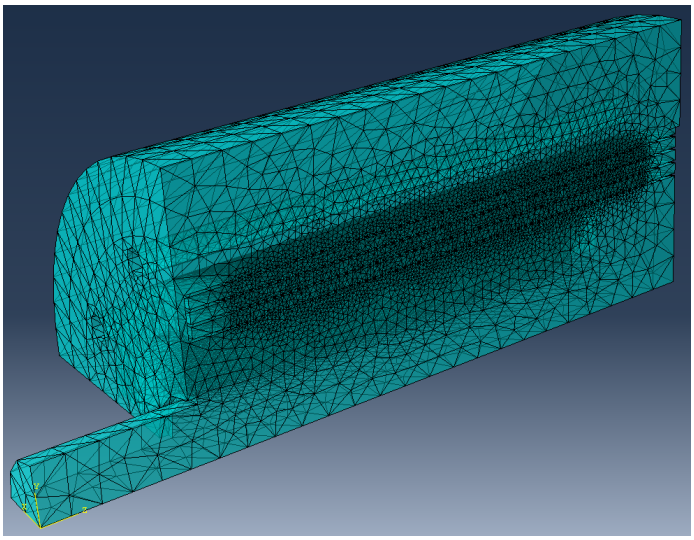

(b) Transparent view of the mesh for the CFD model.

Figure 4.12: Solid and transparent view of the mesh generated in the CFD simulation.

Step definition

The step parameters set up for this simulation was what is referred to as a flow step in Abaqus. The minimum step increment was set initially to 0.001 seconds and the total step length was set to one second. This setup meant a minimum of one thousand step increments had to be calculated in order to complete the simulation. However, due to the complex nature of the airflow, it was expected that most of the step increments would have to be smaller than the specified step increment in order to complete the simulation. Consequently, more increments had to be calculated in order to complete the simulation.

Load case and boundary conditions

In the CFD model, the boundary conditions were the two constraints for the inlet and the outlet of the model. The outlet was constrained by setting the pressure at the outer surface of the CFD model to 1 atm or 0.101 MPa. The inlet of the CFD model was constrained by setting the velocity of the airflow to be 486.7 m/s, as was found by Lloyd's Register ODS[16]. The sides of the CFD model which coincides with the yz- and xz plane were set to be symmetry planes in the simulation.

4.3.3 Optimisation of the model

Since the initial attempt to run the simulation resulted in an error message regarding too many elements, the number of elements had to be reduced substantially. One solution could be to increase the size of the mesh in the model. This modification would reduce the number of elements, but since some of the sections of the air domain are quite thin, a finer mesh is needed in these areas. Other disadvantages with using a coarser mesh would be that the results of the simulation would not be as accurate. Another option would be to look at possible symmetries in the model in order to reduce the size of the model. This model reduction would significantly reduce the number of elements in the model and at the same time not impact the accuracy of the simulation since the mesh size could have been kept as it originally was. Considering these advantages and disadvantages, the model was reduced in size by utilising the symmetries about the xz-, and yz plane in the same manner as was done for the diffusor model.

4.4 Initial version vs final version

Initially it was intended to run both the CFD simulation and the dynamic explicit simulation in parallel in Abaqus. This method is a strategy called co-simulation, which is where Abaqus calculates one step increment for the first simulation, reads the pressure values for every node in the simulation and applies that pressure as an input for the second simulation for every step increment. Using this method, it is possible to see how a structure will react to the loads imposed by the flow through the component, and how the flow will change

because of the deformed component. The disadvantage with this method is that it requires Abaqus to recalculate the displacements of the component for each iteration it runs, which requires a lot more computer power and memory. The original models were linked using a co-simulation boundary between the CFD model and the diffusor model. This boundary would be every surface that was common for both models, i.e. the surfaces where the airflow was in contact with the diffusor. The initial attempts were run for a few increments and it was estimated that completing the co-simulation would take several months with the computer available, and this approach was thus quickly discarded as a strategy suitable for this thesis.

Since co-simulation would not be feasible for this analysis, it was decided to run both simulations separately and apply the results from the CFD simulation as an input for the diffusor simulation manually. Thus, the co-simulation boundary condition of both models were no longer needed and was deleted from the models.

Chapter 5

Results

In this section, the results from the CFD- and the dynamic explicit simulation will be presented.

5.1 CFD results

The CFD simulation ran for approximately two weeks on the computer previously mentioned in Section 3.2. In this subsection, the results from the CFD simulation will be presented and they are ordered in three subsections. The initial step, vortex flow, which is approximately 0.0016 seconds into the simulation, and fully developed flow, which was at approximately 0.006 seconds into the simulation.

5.1.1 Initial step

At the initial step, at t=0, the pressure levels at the outlet of the model was defined to be 1 atm, or 0.101 MPa and the velocity of the flow at the inlet was defined to be 486.7 m/s as reported in the report by Lloyd's Register ODS[16]. The pressure distribution is shown in Figure 5.1 and the velocity distribution is shown in Figure 5.2 below. Figure 5.1 shows that the pressure at the inlet apparently was negative at the initial step, as the pressure at this location could not be defined along with the velocity of the flow. This situation was accepted, as it was a fairly low negative pressure of only 0.082 MPa at the inlet.

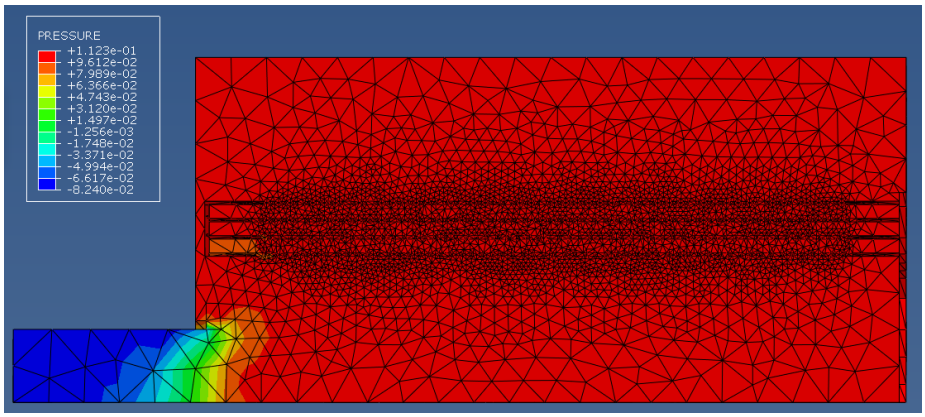

Figure 5.1: The pressure levels in the diffusor at the beginning of the simulation.

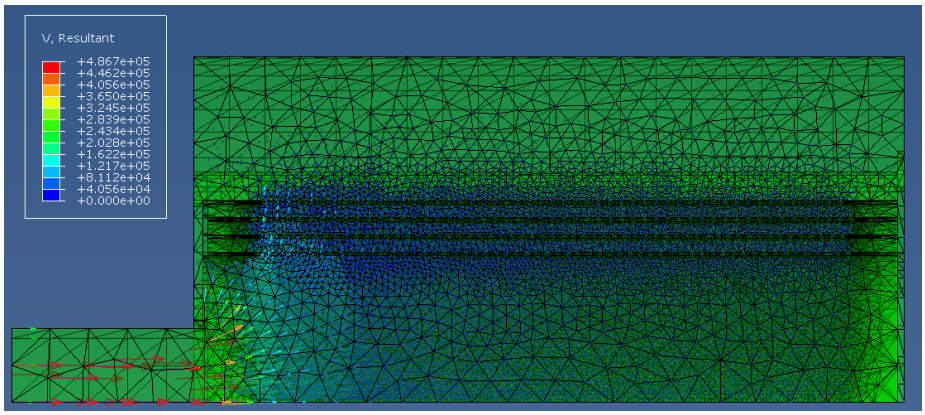

Figure 5.2: The velocity levels in the diffusor at the beginning of the simulation.

5.1.2 Vortex flow

As the flow begins to develop over time, an initial vortex flow is observed in the diffusor. This behaviour was observed during the initial stages of the flow development. In Figure 5.3 the pressure distribution is shown, where one can see pockets of air with lower pressure than the surrounding air. The highest pressures are still found near the top plate of the diffusor as most of the air is pushed there from the inlet flow. In Figure 5.4 the velocity distributions of the diffusor is shown during the same time period as Figure 5.3. It is clearly seen that the low pressure zones in Figure 5.3 coincides with the centre of the vortices seen in Figure 5.4.

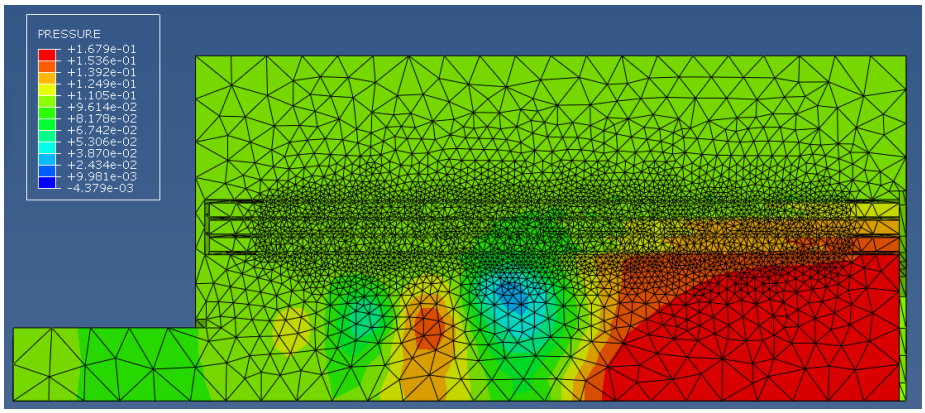

Figure 5.3: The pressure distribution in the diffusor during the early stages of the flow development, where pockets of low pressure air is observed.

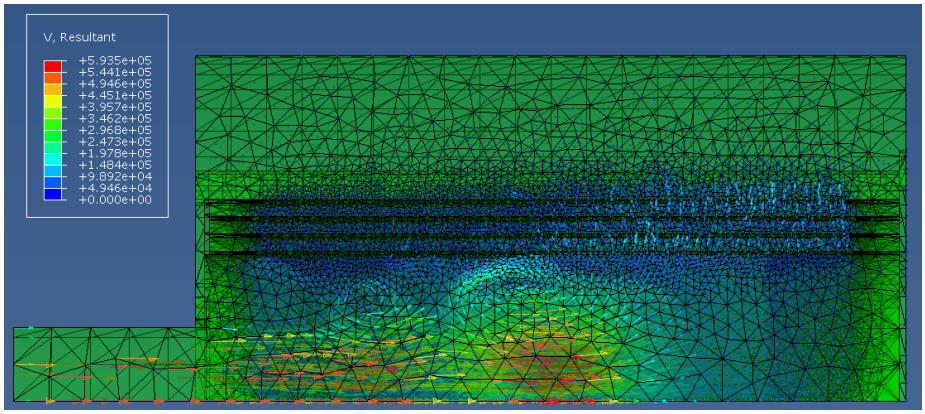

Figure 5.4: The velocity distribution in the diffusor during the early stages if flow development. The vortices are more clearly shown here.

5.1.3 Fully developed flow

After the flow through the diffusor had been developed, a stable flow situation was observed over the time period of the simulation. In Figure 5.5, the pressure distribution of the diffusor is shown, where it can be observed some small pressure fluctuations in the inlet flow of the diffusor. The pressure levels of the diffusor are highest at the top plate, where the airflow hits the plate. Figure 5.6 shows the velocity distribution of the diffusor, and one can see that the vortex behaviour apparent in Figure 5.4 is over. Now a more linear flow through the diffusor is seen, where most of the air hits the top plate before being dissipated out through the perforated plates.

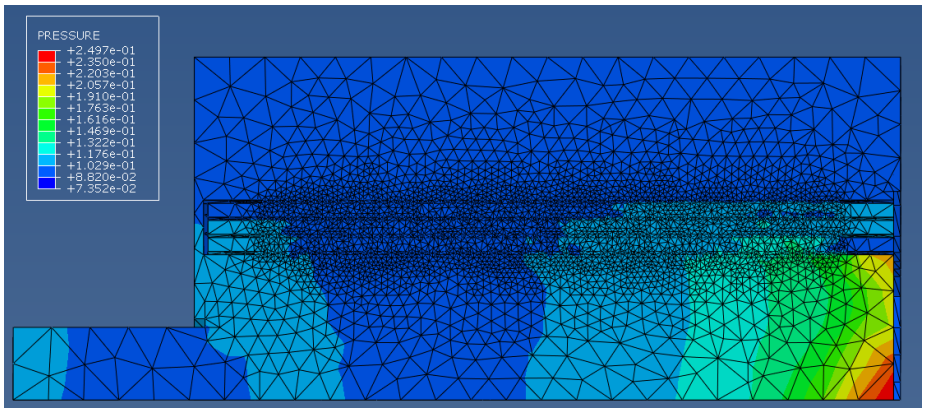

Figure 5.5: The pressure distribution in the diffusor after the vortex flow has ended and a more linear flow is observed.

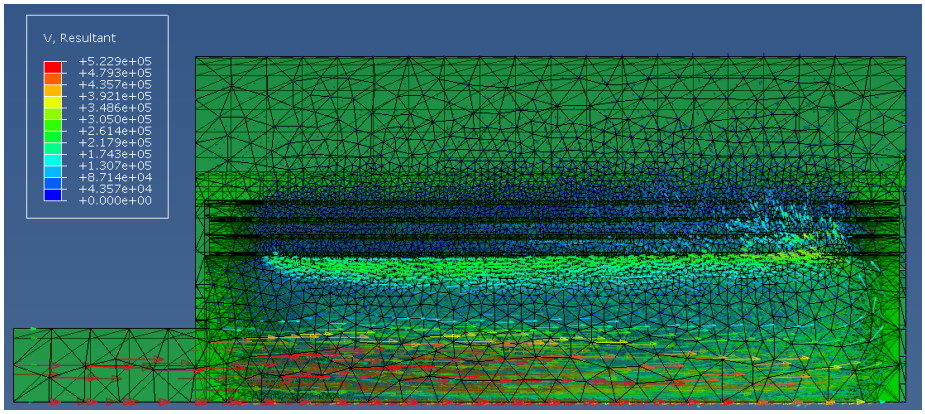

Figure 5.6: The velocity distribution in the diffusor after the vortex flow has ended and a more linear flow is observed.

5.1.4 Pressure development

The pressure levels in the diffusor was collected and exported to Excel in order to graph the developments of the pressure on the different parts of the diffusor. The results of the pressure development during the simulation is shown in Figure 5.7. Note that in Figure 5.7, the perforated plates are numbered one to four, where plate one is the innermost plate and plate four is the outermost plate. Furthermore, the pressure readings are further denoted with brackets, where [inlet] and [outlet] denotes whether the pressure readings were taken from near the inlet or the top plate.

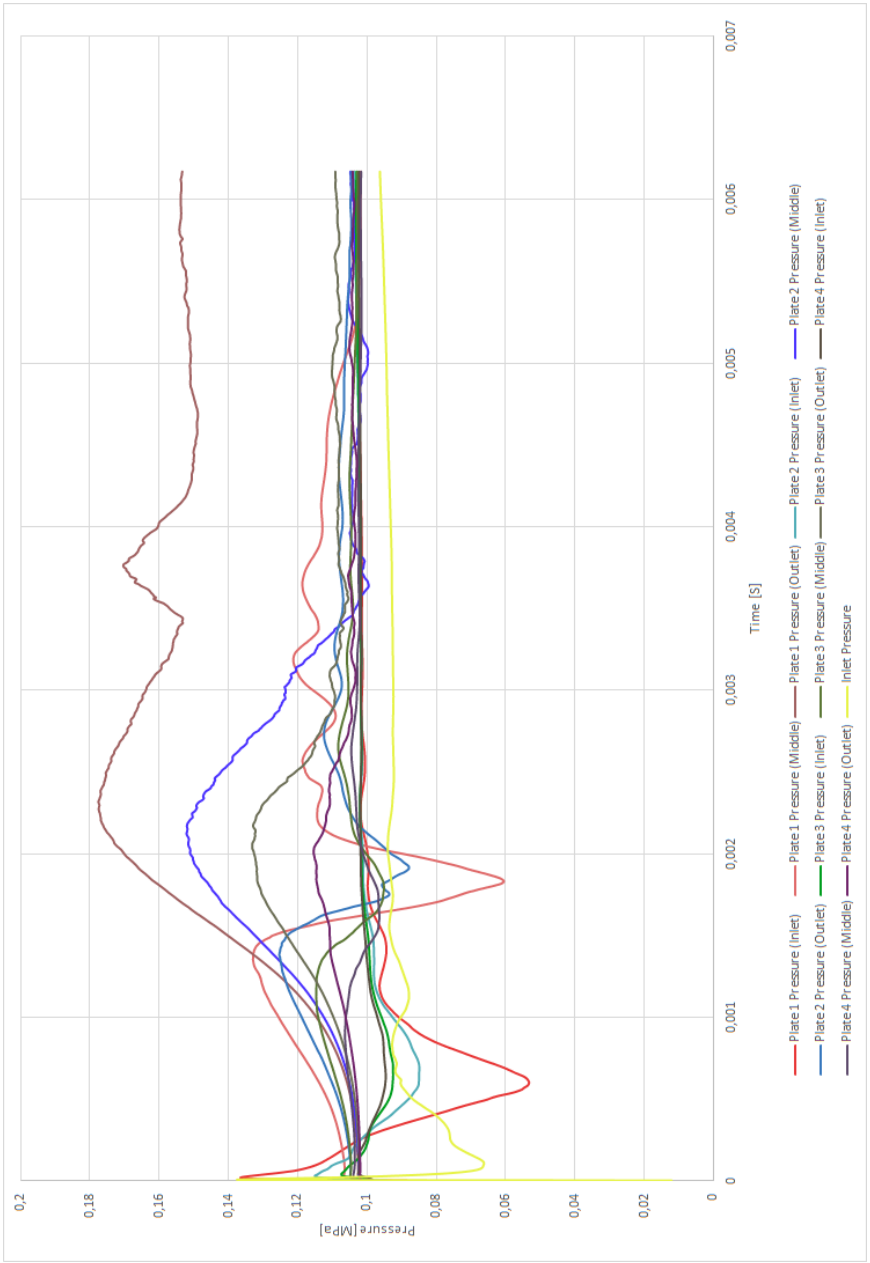

Figure 5.7: Pressure readings from the CFD simulation.

5.2 Diffusor results

The standard explicit diffusor simulation ran for approximately two weeks on the computer previously specified in Section 3.2.

5.2.1 Initial step

At the initial step of the simulation, there are no stresses or strains in the model, as would be expected. This situation is shown in Figure 5.8. This figure is included in order to verify that no stresses were induced by any of the boundary conditions before the simulation had started.

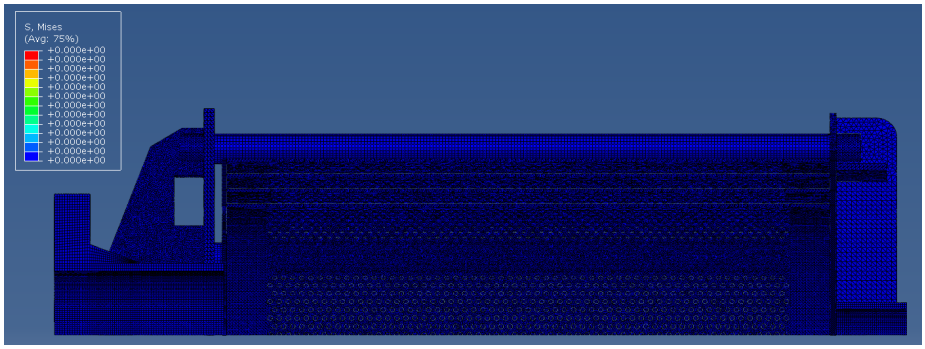

Figure 5.8: The initial step of the diffusor simulation.

5.2.2 Maximum load

When the loads applied on the diffusor is at their highest magnitude, the diffusor results have stress concentrations at the top and bottom of the perforated plates as shown in Figure 5.9. In addition, the top plate shows signs of transferring some stresses to the top radial plates.

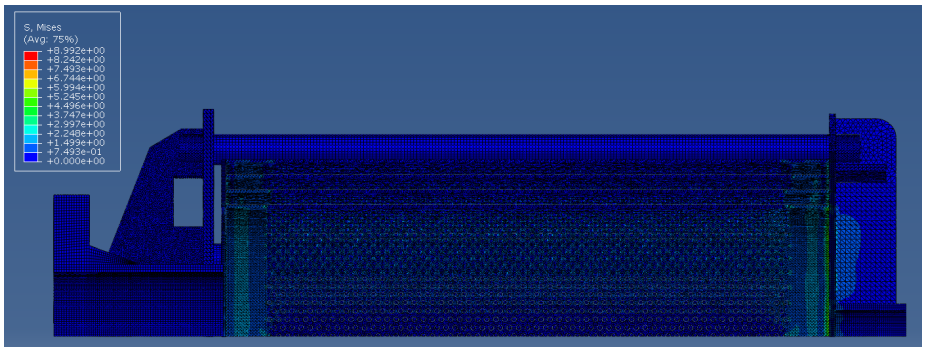

Figure 5.9: The Von Mises stresses for the step with the highest load in the diffusor simulation.

5.3 Post processing in Link-PFAT

As explained in Section 3.3, the resulting ODB-file of the diffusor simulation was imported into Link-PFAT and set up with the various settings outlined in Section 3.3. The resulting cycles to failure, output by Link-PFAT is displayed in Table 5.1 below.

Part name	Eff. Stress Amplitude [MPa]	Component Lifetime Cycles
Top Plate	9.38	$1.62 \cdot 10^{13}$
Perforated plate 1	8.77	$2.31 \cdot 10^{13}$
Perforated plate 2	6.97	$7.79 \cdot 10^{13}$
Perforated plate 3	6.11	$1.57 \cdot 10^{14}$
Perforated plate 4	5.13	$3.95 \cdot 10^{14}$
Top radial plate 1	2.91	$7.92 \cdot 10^{15}$
Top radial plate 2	5.09	$5.76 \cdot 10^{15}$
Welding plate	1.32	$5.09 \cdot 10^{17}$
Top pipe	1.23	$7.55 \cdot 10^{17}$
Crown	0.79	$7.55 \cdot 10^{18}$
Supporting rod 1	0.37	$4.12 \cdot 10^{20}$
Supporting rod 2	0.37	$4.09 \cdot 10^{20}$
Bottom radial plate 1	$5.76 \cdot 10^{-6}$	$1.15 \cdot 10^{46}$
Bottom radial plate 2	$6.81 \cdot 10^{-6}$	$4.74 \cdot 10^{45}$
Bottom plate	$1.57 \cdot 10^{-6}$	$1.10 \cdot 10^{49}$
Pipe inlet	$1.85 \cdot 10^{-10}$	$6.71 \cdot 10^{69}$

Table 5.1: The resulting cycles to failure for the different components of the diffusor. Here, the perforated plates are numbered, where number 1 is the innermost plate and number 4 is the outermost plate.

5.4 Lifetime of the components

The cycle defined in the analysis represents one pressure spike in the flow through the diffusor. As discovered in the report by Lloyd's Register ODS[16], this pressure spike occurs with a frequency of up to 1000 Hz during operation. This would mean that every second that the diffusor is in operation, 1000 pressure spikes of the same type that have been simulated in this analysis will pass through the diffusor. If one assumes the worst case scenario, where the CDP valve is continuously in its opened state, meaning that the airflow would pass through the diffusor continuously 24 hours per day, this would correspond to a worst case scenario of $3.15 \cdot 10^{10}$ cycles per year.

5.5 Specific lifetime

Using the yearly cycle count of $3.15 \cdot 10^{10}$ cycles per year, the total lifetime of the components can be calculated. The results of this calculation is shown in Table 5.2 below.

Part name	Component Lifetime Years
Top Plate	513.5
Perforated plate 1	732.2
Perforated plate 2	2 469,2
Perforated plate 3	4 976.4
Perforated plate 4	12 520.2
Top radial plate 1	251 133.5
Top radial plate 2	182 573.4
Welding plate	$1.61 \cdot 10^{7}$
Top pipe	$2.39 \cdot 10^{7}$
Crown	$2.39 \cdot 10^{8}$
Supporting rod 1	$1.31 \cdot 10^{10}$
Supporting rod 2	$1.30 \cdot 10^{10}$
Bottom radial plate 1	$3.65 \cdot 10^{35}$
Bottom radial plate 2	$1.5 \cdot 10^{35}$
Bottom plate	$3.49 \cdot 10^{38}$
Pipe inlet	$2.13 \cdot 10^{59}$

Table 5.2: The resulting fatigue lifetimes for the different components of the diffusor. Here, the perforated plates are numbered, where number 1 is the innermost plate and number 4 is the outermost plate.

Chapter 6

Discussion and further work

The pressure and velocity results for the CFD simulation, presented in Section 5.1.3 above, coincides with the results from the report done by Lloyd's Register ODS[16]. This result means that the boundary conditions of the model are defined correctly and that the pressure readings taken from the CFD simulation should be correct in regard to the real world conditions of the diffusor.

The use case specified in Section 5.4 may seem unrealistic as the CDP valve would be constantly open and air would pass through the diffusor at all times with this use case. However, operators have been using the bleed assembly to regulate the speed of the turbine, despite other systems designed for this purpose being in place, and as Mjørud has no data on how often this operation occurs, the worst-case scenario is assumed. This situation is naturally not the case as the turbine would choke in this scenario, but as the concern of this thesis is the fatigue life of the diffusor, it is better to be conservative, as in most fatigue life calculations, and assume a worse use case than in real life.

As is shown in Section 5.5, the lifetimes of the different components cover a very wide range, from 513.5 years to $2.13 \cdot 10^{59}$ years. Even if using a safety factor of 2, the minimum lifetime of the diffusor would be 256.75 years. This result exceeds the 20-year requirement of Mjørud by over 12 times. It can be seen that all the parts of the diffusor where the pressures have been defined have a significantly lower lifetime than the components where the pressure have not been defined. This distribution is a natural consequence of the pressure definitions applied in the model, since the parts subjected to no pressure at all would only experience the resulting forces distributed by the diffusor itself. If the diffusor was to be analysed again and more pressure values on the components were wanted, the co-simulation feature of Abaqus, outlined in Section 4.4, would be a good method for analysing the diffusor. However, as already mentioned, that would require a substantial amount of computer power. Another way to get more complete results would have been to take pressure readings manually from all the parts during the data gathering from the CFD simulation, as this would

apply a load to each component. However, the components that were not given a pressure load applied to them were as previously mentioned not regarded as having a high risk of failure due to their history in previous diffusors outlined in Section 1.1.

Another limitation of this analysis is the lack of modal analysis of the diffusor, in order to evaluate any effects stemming from resonance frequencies. If the diffusor has a resonance frequency close enough to 1000 Hz, one would expect that the diffusor would experience more severe stresses due to this amplifying effect caused by resonance. One recommendation for further work is to perform a modal analysis to see how the diffusors' frequency response is in order to further refine the results.

The high fatigue life of the components could also be misleading as not all thermal effects are considered in this thesis, as mentioned in Section 4.2.5. The reason that thermal expansion was omitted from this thesis was that the diffusor was assumed to not be subjected to a high number of temperature fluctuations during normal operation since the diffusor is placed in the exhaust duct of the gas turbine. Thus, there would not be a high impact on the fatigue life because of thermal expansions. However, the thermal expansion, outlined in Section 2.5, could have made an impact to the fatigue life as the temperature increase from room temperature to operating temperature would have induced a thermal strain in the diffusor when starting the gas turbine after installation of the diffusor. This situation would affect the fatigue life of the diffusor negatively, since the diffusor would be pre-stressed due to thermal expansion.

Other factors that have impacted the calculated lifetime was the implementation of Goodmans method as a mean stress correction model. This model is known to be somewhat inaccurate, but usually conservative. And thus this implementation should have led to a lower expected lifetime, but this effect seems to have been outweighed by other effects or inaccuracies.

Other considerations to keep in mind is that the welds of the diffusor have not been evaluated or considered in this thesis. The reason this omission was done was primarily since the welds had been improved from the previous iterations, and thus was not considered to be a high risk area of this diffusor. It was also done partly due to time constraints and partly due to lack of material data for the welding material used to weld the components of the diffusor to each other. It is recommended to perform a fatigue life analysis for the welds in the diffusor as well in order to determine whether the welds will fail due to fatigue before the individual components of the diffusor will fail.

Since the diffusor is placed in a relatively extreme environment, it could be reasonable to expected that the steel could behave differently than the test environment that fatigue tests are performed in. Usually, these tests are done at room temperature, probably since the testing devices could give incorrect

readings at elevated temperatures. As previously mentioned, the article by Chopra [14] stated that the fatigue life of austenitic stainless steel does not depend on temperature up to 427 °C. Despite this statement, the thermal fatigue should still not be disregarded in future work, especially since the temperature could at some times exceed the 400°C specified for this analysis.

Furthermore, other factors that could have impacted the fatigue life was that gravity was not defined in the simulation. The inclusion of gravity would also lead to the diffusor being pre-stressed due to forces imposed by gravity, and could thus reduce the fatigue life for certain components in the diffusor.

Other aspects of the analysis that could have been done if more time was available would be to prepare the model in order to be run using Vilje, a supercomputer available for certain research[26]. When it was discovered that the initial model would be too complex to be run on the hardware available, there was not enough time to implement the changes needed to run the simulation on a supercomputer. Instead, as already mentioned in Section 4.4, the model was separated into two different simulations in order to at least get the simulation to complete the analysis. If it were decided to utilise a supercomputer instead of an enterprise computer in order to perform the simulation, there would be a chance that more errors with the model would be encountered due to this change. As a lot of the time allotted had already been spent in order to get the model to run without encountering any errors using an enterprise computer, it was not deemed time efficient enough to make this change. If, however, the utilisation of a supercomputer had been planned from the beginning of the thesis, a co-simulation would have been possible, which in turn could have led to more realistic results. It would also have been possible to perform multiple simulations if the need for changes in the components of the diffusor was discovered. Since the diffusor encounters a varying pressure load during operation, perhaps a more complete representation of the pressure levels is needed in order to fully be able to accurately calculate the fatigue life of the diffusor. Since the co-simulation feature of Abaqus allows for precisely this level of detail regarding the pressure levels in the entire diffusor simultaneously, implementing a co-simulation method for further work while using a supercomputer would be a large improvement for this analysis.

If more time had been available in order to model the diffusor, this time would have been spent on partitioning the components in order to utilise a different mesh element, as tet-elements are generally considered to be less suited for complex parts[22]. A different mesh element could have contributed to more accurate results for the fatigue life of the components.

6.1 Conclusion

The main purpose for this thesis was to perform a fatigue life analysis of the diffusor currently installed at several oil- and gas platforms. As several iterations of the diffusor had already been manufactured, an overview of the different iterations was assembled in order to better understand the problem encountered with the diffusor. In order to perform the fatigue life analysis, two FEM models were created.

A CFD model was created in order to analyse the behaviour of the airflow inside the diffusor and to collect pressure readings from specific points on several selected components of the diffusor. These components, namely the perforated plates and the top plate, were selected for closer inspection as they had been problem areas in previous iterations of the diffusor and warranted some extra attention due to this issue.

A standard explicit model was created in order to analyse the mechanical response of the diffusor as a result of the pressures, applied by the airflow, obtained from the CFD analysis. During the creation of the standard explicit model, all of the components of the diffusor had to be recreated in Abaqus in order to create a functioning model. Parts of particular importance in this regard were the perforated plates, where holes had to be modelled into the plates in order to get the correct behaviour of the diffusor, as was intended by Mjørud AS.

The creation of the different FEM simulations proved to be more difficult than first envisioned, as the diffusor consisted of many complex parts, with challenging geometry, which had to be recreated as accurately as possible in order to have confidence in the results of the simulation. As the diffusor models became more complicated than both Abaqus and the available computer was able to handle, the models had to be simplified in order to be able to complete the analysis. These simplifications included utilisation of symmetry and omission of welds.

The fatigue life of the component with the lowest lifetime was found to be the top plate of the diffusor, with a somewhat unrealistic lifetime of 513.5 years. Thus, the diffusor would last a minimum of 513.5 years until it would break due to fatigue. This lifetime omits the possibility of whether the welding seams of the diffusor would break first and is left to further examination.

Overall, the general perception during this thesis has been that fatigue life evaluation of complex components with complex load cases was more involved and computationally expensive than first envisioned. Extensive knowledge of both fatigue behaviour of materials and computational implementation of such analysis is vital in order to adequately perform this kind of fatigue analysis.

References

[1] Møller K.R. *Åsgård B, Main Generator A, Sound and Vibration measurements July 2011*. Loyd's Register ODS, 2011.

[2] NORSOK. *S-002, "Working environment" rev.4 (Lysaker, Norway)*. 2004. URL: http://www.standard.no/en/sectors/energi-og-klima/petroleum/norsok-standard-categories/s-safety-she/s-0021/ (visited on 06/07/2018).

[3] NORSOK. *M-001, "Materials Selection" fifth ed. (Lysaker, Norway)*. 2014. URL: http://www.standard.no/fagomrader/energi-og-klima/petroleum/norsok-standard-categories/m-material/m-0015/ (visited on 06/28/2018).

[4] Sines G., Waisman J.L., Dolan T.J. *Metal fatigue*. McGraw-Hill, 1959, pp. 145–169.

[5] Dowling N.E. *Mechanical Behavior of Materials: Engineering Methods for Defoemation, Fracture, and Fatigue*. 4th ed., international ed. contributions by Prasad K.S., Narayanasamy R. Pearson Education, 2013.

[6] Callister W.D., Rethwwisch D.G. *Materials Science and Engineering*. 8th ed., SI version. Wiley, 2011.

[7] Hibbeler R.C. *Mechanics of materials*. 8th ed. in SI Units. Prentice Hall, 2011.

[8] Ross C. *Mechanics of solids*. Prentice Hall, 1996.

[9] Society of Automotive Engineers & American Society for Testing Materials. *Metals and alloys in the unified numbering system*. ASTM International, 2008.

[10] Solomon N., Solomon I. "Effect of deformation-induced phase transformation on AISI 316 stainless steel corrosion resistance". In: *Engineering Failure Analysis* 79 (2017), pp. 865–875.

[11] Desu R.K. et al. "Mechanical properties of austenitic stainless steel 304L and 316L at elevated temperatures". In: *Journal of Materials Research and Technology* 5.1 (2016), pp. 13–20.

[12] *Elevated temperature physical properties of stainless steels*. 2016. URL: https://www.bssa.org.uk/topics.php?article=139 (visited on 06/25/2018).

[13] Mohammad K.A. et al. "Fatigue behavior of Austenittic Type 316L Stainless Steel". In: *IOP Conference Series: Materials Science and Engineering* 36.1 (2012), p. 012012.

[14] Chopra O.K. "Development of a Fatigue Design Curve for Austenitic Stainless Steels in LWR Environments: A Review". In: *ASME 2002 Pressure Vessels and Piping Conference* (2002), pp. 119–132.

[15] Bell K. *An engineering approach to finite element analysis of linear structural mechanics problems*. eng. Trondheim, 2013.

[16] Gullman-Strand J. *Åsgård B, Main Generator A, CFD analysis of Exhaust Collector bleed flow*. Loyd's Register ODS, 2011.

[17] *FEM post-processor for fatigue analysis*. 2018. URL: https://www.sintef.no/en/software/fem-post-processor-for-fatigue-analysis/ (visited on 10/22/2018).

[18] SINTEF. *LINKpfat User Manual, Version 1.4.1.59*. SINTEF, 2018.

[19] Goodman J. *Mechanics Applied to Engineering*. London: Longman, Green & Company, 1899.

[20] *Inventor | Mechanical Design & 3D CAD Software | Autodesk*. 2018. URL: https://www.autodesk.eu/products/inventor/overview (visited on 11/25/2018).

[21] *Abaqus Unified FEA - Simulia™by Dassault Systems®*. 2018. URL: https://www.3ds.com/products-services/simulia/products/abaqus/ (visited on 11/25/2018).

[22] Wang E., Nelson T., Rauch R. "Back to elements-tetrahedra vs. hexahedra". In: *Proceedings of the 2004 international ANSYS conference* (2004).

[23] Engineering Toolbox. *Air - Density, Specific Weight and Thermal Expansion Coefficient at Varying Temperature and Constant Pressures*. 2003. URL: https://www.engineeringtoolbox.com/air-density-specific-weight-d_600.html (visited on 06/15/2018).

[24] Hilsenrath J. et al. "Tables of Thermal Properties of Gases". In: *Journal of the Electrochemical Society* 103.5 (1956). ISSN: 0013-4651.

[25] Engineering Toolbox. *Air - Thermal Conductivity*. 2009. URL: https://www.engineeringtoolbox.com/air-properties-viscosity-conductivity-heat-capacity-d_1509.html (visited on 06/15/2018).

[26] *Vilje | Sigma2*. 2012. URL: https://www.sigma2.no/content/vilje (visited on 11/23/2018).

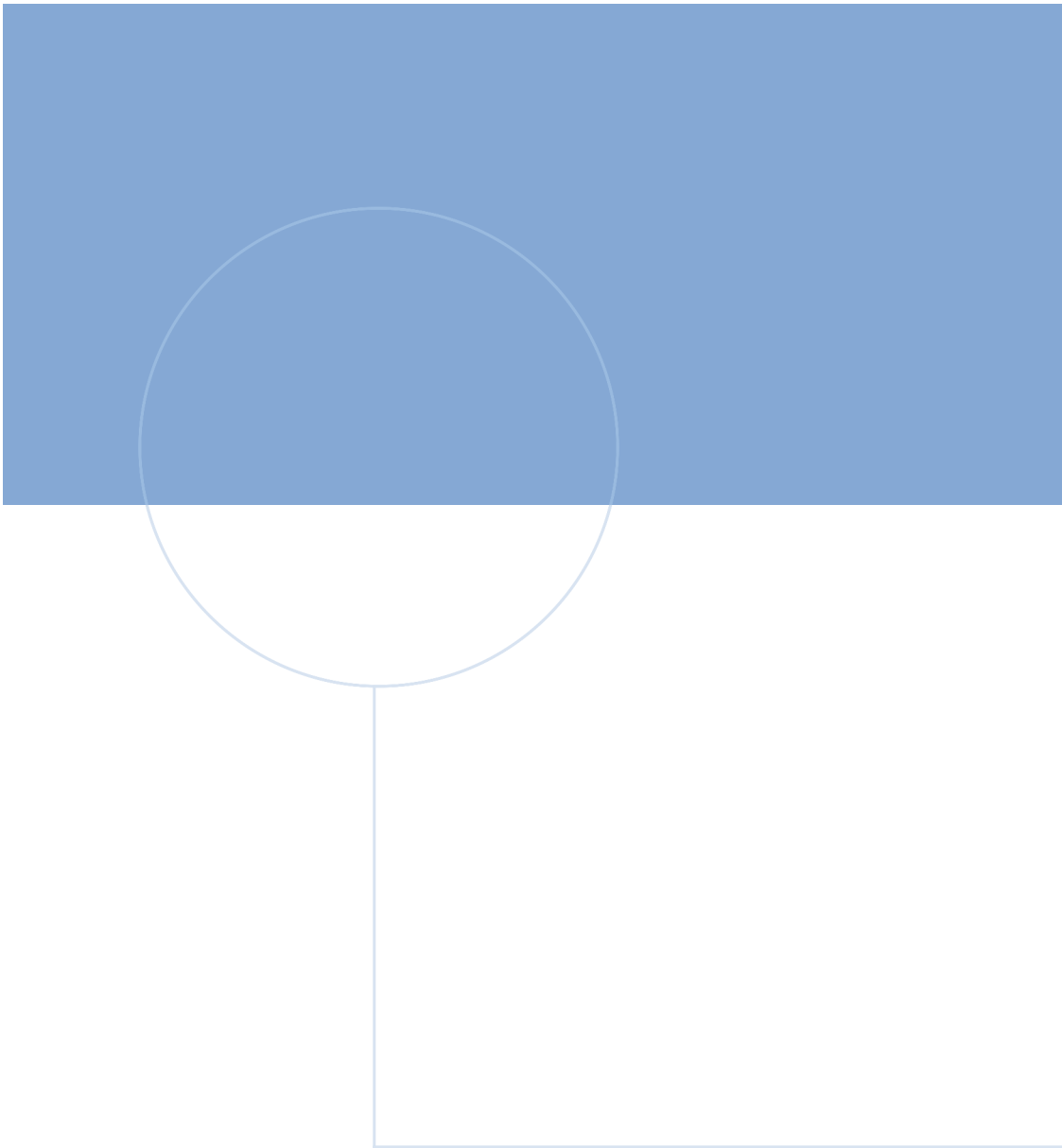

NTNU
Norwegian University of
Science and Technology

Mjørud